Article

Cell Reports

Mechanistic Differences in Neuropathic Pain Modalities Revealed by Correlating Behavior with Global Expression Profiling

Graphical Abstract

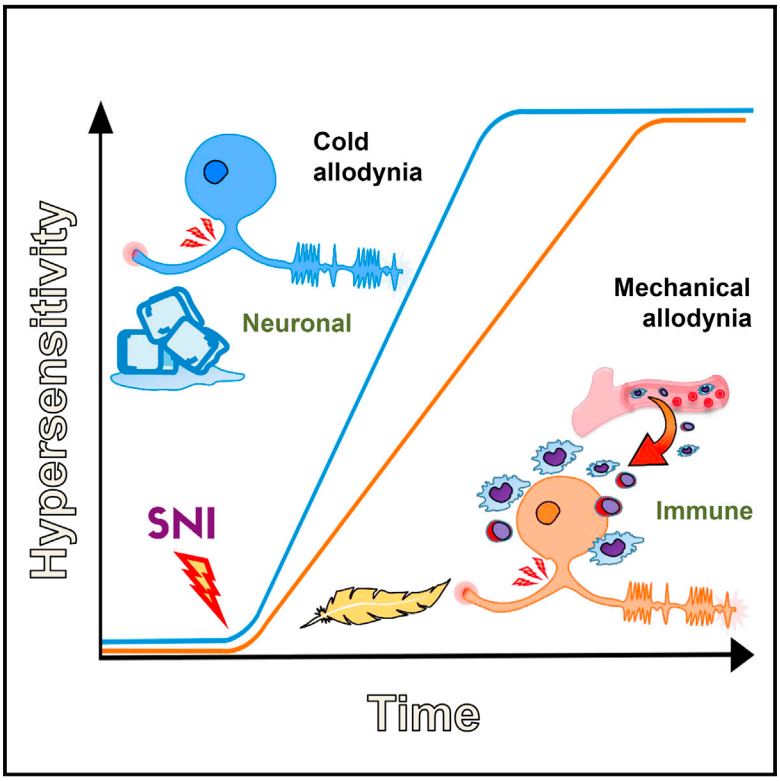

Authors

Enrique J. Cobos, Chelsea A. Nickerson, Fuying Gao, ..., Manu Rangachari, Clifford J. Woolf, Michael Costigan

Correspondence

michael.costigan@childrens.harvard.edu

In Brief

Cobos et al. correlated gene expression with behavior after nerve injury and found that two distinct processes contribute to neuropathic pain: one that occurs in neurons, leading to cold allodynia, and another that includes immune cells and neurons, leading to tactile allodynia.

Highlights

- Peripheral processes leading to neuropathic cold and tactile allodynia differ
- TrpV1-lineage neurons participate in cold, but not tactile, allodynia
- Immune system activation contributes to tactile allodynia but minimally to cold allodynia

Data and Software Availability

GSE102937

Cobos et al., 2018, Cell Reports *22*, 1301–1312
January 30, 2018
https://doi.org/10.1016/j.celrep.2018.01.006

CellPress

Cell Reports
Article

Mechanistic Differences in Neuropathic Pain Modalities Revealed by Correlating Behavior with Global Expression Profiling

Enrique J. Cobos,[1,2,3] Chelsea A. Nickerson,[1] Fuying Gao,[4] Vijayendran Chandran,[4,5] Inmaculada Bravo-Caparrós,[2] Rafael González-Cano,[1] Priscilla Riva,[1] Nick A. Andrews,[1] Alban Latremoliere,[1] Corey R. Seehus,[1] Gloria Perazzoli,[2,6] Francisco R. Nieto,[2,3] Nicole Joller,[7] Michio W. Painter,[1] Chi Him Eddie Ma,[1] Takao Omura,[1] Elissa J. Chesler,[8] Daniel H. Geschwind,[4] Giovanni Coppola,[4] Manu Rangachari,[7,9,10] Clifford J. Woolf,[1] and Michael Costigan[1,11,12,*]

[1]Kirby Neurobiology Center, Boston Children's Hospital and Department of Neurobiology, Harvard Medical School, Boston, MA 02115, USA
[2]Department of Pharmacology and Institute of Neuroscience, Faculty of Medicine and Biomedical Research Center, University of Granada, 18071 Granada, Spain
[3]Biosanitary Research Institute, University Hospital Complex of Granada, 18012 Granada, Spain
[4]Department of Neurology, David Geffen School of Medicine, University of California, Los Angeles, Los Angeles, CA 90095, USA
[5]Department of Pediatrics, School of Medicine, University of Florida, Gainesville, FL 32610-0296, USA
[6]Department of Anatomy and Embryology, School of Medicine, University of Granada, 18071 Granada, Spain
[7]Center for Neurologic Diseases, Brigham and Women's Hospital, Harvard Medical School, Boston, MA 02115, USA
[8]The Jackson Laboratory, 600 Main Street, Bar Harbor, ME 04609, USA
[9]Department of Neurosciences, Centre de recherche du CHU de Québec, Université Laval, Québec, QC, Canada
[10]Department of Molecular Medicine, Faculty of Medicine, Université Laval, Québec, QC G1V 0A6, Canada
[11]Department of Anesthesia, Boston Children's Hospital, Harvard Medical School, Boston, MA 02115, USA
[12]Lead Contact
*Correspondence: michael.costigan@childrens.harvard.edu
https://doi.org/10.1016/j.celrep.2018.01.006

SUMMARY

Chronic neuropathic pain is a major morbidity of neural injury, yet its mechanisms are incompletely understood. Hypersensitivity to previously non-noxious stimuli (allodynia) is a common symptom. Here, we demonstrate that the onset of cold hypersensitivity precedes tactile allodynia in a model of partial nerve injury, and this temporal divergence was associated with major differences in global gene expression in innervating dorsal root ganglia. Transcripts whose expression change correlates with the onset of cold allodynia were nociceptor related, whereas those correlating with tactile hypersensitivity were immune cell centric. Ablation of TrpV1 lineage nociceptors resulted in mice that did not acquire cold allodynia but developed normal tactile hypersensitivity, whereas depletion of macrophages or T cells reduced neuropathic tactile allodynia but not cold hypersensitivity. We conclude that neuropathic pain incorporates reactive processes of sensory neurons and immune cells, each leading to distinct forms of hypersensitivity, potentially allowing drug development targeted to each pain type.

INTRODUCTION

Peripheral neuropathic pain in animal models is associated with hypersensitivity to noxious and non-noxious stimuli in areas of tissue that neighbor those normally innervated by the damaged nerves. Changes both in the peripheral nervous system (PNS) and central nervous system (CNS) contribute to the development of this pain hypersensitivity (Costigan et al., 2009b). Global gene expression studies in the adult rodent dorsal root ganglia (DRG) in response to sciatic nerve injury have helped define the peripheral mechanisms likely to contribute to the changes in neuropathic pain-like hypersensitivity (Costigan et al., 2009b; LaCroix-Fralish et al., 2011), as well as novel targets for therapy (Dib-Hajj and Waxman, 2014; Tegeder et al., 2006).

Following sciatic nerve injury, the ipsilateral L3-5 lumbar DRGs contain the cell bodies of injured and non-injured primary sensory neurons, satellite cells, fibroblasts, and blood vessels, as well as resident immune cells and those recruited from the blood (Hu et al., 2007). Peripheral nerve injury induces transcriptional changes in each of these diverse cell types (Costigan et al., 2002, 2010; Watkins and Maier, 2002). Peripheral nerve injury induces pain-like hypersensitivity in rodents that develops over the first week or so following the axonal damage (Colleoni and Sacerdote, 2010; Jaggi et al., 2011). Here, we have determined the onset of two chronic pain-like sensory modalities (tactile and cold allodynia) in C57BL/6 mice at high temporal resolution (daily) over the first 10 days in the spared nerve injury (SNI) model (Decosterd and Woolf, 2000), and we found clear differences in their temporal evolution, with cold sensitivity developing quicker than tactile allodynia. The temporal separation of these two clinically important neuropathic pain modalities (Jensen and Finnerup, 2014) led us to design a global gene expression study in lumbar DRGs ipsilateral to the nerve injury to directly correlate the relative timing of transcript expression and sensory modality changes.

We demonstrate differences in the kinetics of early neuronal and late immune gene regulation events, changes which closely

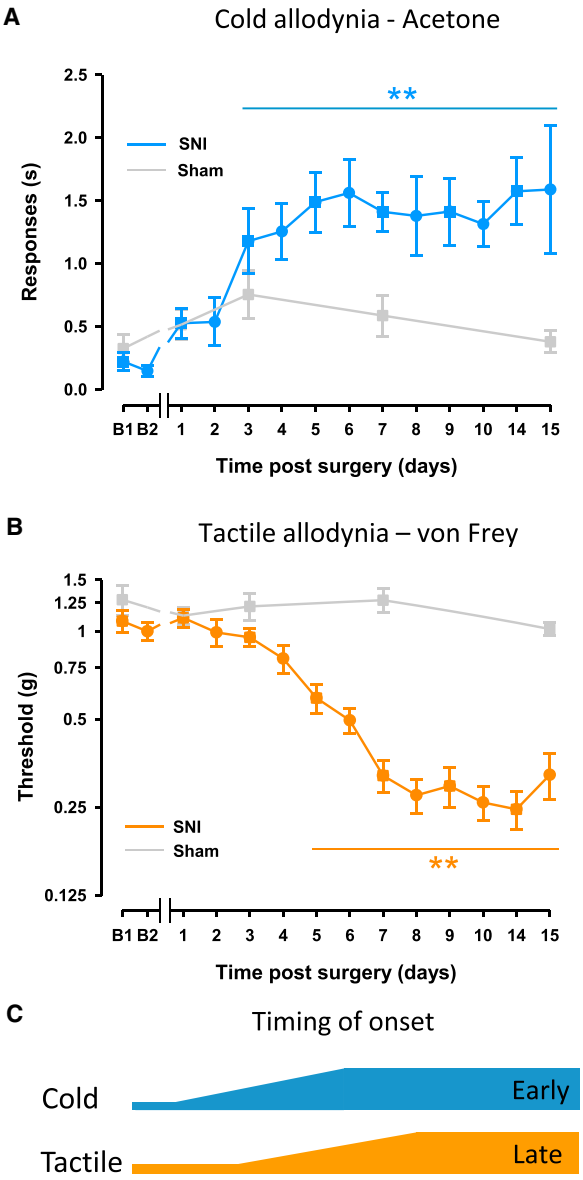

Figure 1. Differences in the Onset of Cold and Tactile Allodynia

(A and B) Cold allodynia (A) develops relatively quickly post-injury, whereas tactile allodynia (B) develops at a slower pace.

(C) The onset time of cold hypersensitivity is illustrated by the blue line (cold) relative to the later onset of tactile hypersensitivity illustrated by the orange line (tactile).

Statistically significant differences between the values from mice after SNI and their basal measures in (A) and (B); *$p < 0.01$ (one-way repeated-measures ANOVA followed by Bonferroni post hoc test). There were no statistically significant differences between basal measures and values after sham surgery (gray lines, one-way repeated-measures ANOVA). Error bars indicate SEM (n = 13 or 14 per group; see Supplemental Experimental Procedures).

mirror the onset of cold and tactile allodynia respectively. These data indicate that different cellular and molecular mechanisms may be responsible for development of tactile and cold allodynia in the damaged PNS, which we confirmed by selectively targeting the immune and nervous systems. Understanding the differences in pain hypersensitivity features should allow us to develop new therapies tailored to their distinct underlying mechanisms.

RESULTS

Onset of Cold and Tactile Allodynia

Tactile and cold allodynia both develop subsequent to peripheral nerve injury and are major clinical concerns of neuropathic pain patients (Jensen and Finnerup, 2014). A high-density time-course analysis of neuropathic pain-related behavioral onset showed that cold and tactile hypersensitivity developed to maximal levels in the first week after nerve injury and persisted for at least 15 days. Cold allodynia developed relatively quickly, reaching a statistically significant increase at 3 days and achieving peak levels 4–5 days post-SNI (Figure 1A); however, tactile allodynia became established over a slower time frame, with a statistically significant decrease of the mechanical threshold at 5 days and reaching maximal levels 7–8 days post-SNI (Figures 1B and 1C). These data agree with previous reports in which cold allodynia develops faster than mechanical hypersensitivity (Decosterd and Woolf, 2000; Pertin et al., 2007; Wijnvoord et al., 2010). Sham-operated controls did not show alterations in either cold or tactile hypersensitivity (Figures 1A and 1B, respectively).

Transcripts Regulated in the DRG Post-SNI

The differences in the onset time of cold and tactile allodynia led us to consider if these pain modalities may have different mechanisms. To investigate this, we performed an expression array profiling experiment over a similar high-resolution time course to the behavioral studies. We evaluated global gene expression in the ipsilateral DRG daily for the first 10 days post-SNI and also at 8 and 16 hr post-SNI.

We initially assessed changes in gene expression in the DRG over 10 days post-SNI in all 1,704 probes differentially regulated over time between naive and injured conditions (moderated F-statistic, $p < 0.01$; Table S1) by a weighted gene co-expression network analysis (WGCNA) (Parikshak et al., 2015). By employing a module merger step that used Euclidean distance to cluster the average module regulation patterns across time (not shown), we were able to reveal eight distinct expression clusters (clusters I–VIII) comprising 1,699 of the regulated probes (Figure 2) and 5 additional probes that did not fit in any of the eight clusters (Table S1). Ingenuity Pathway Analysis (IPA) of content of each cluster annotated their general functional identity, which delineate the most overrepresented descriptors of gene function assigned to each transcript in each cluster (see "Function/Cell type" and "Example Genes" in Figure 2).

A similarity plot of average gene expression across time for each cluster demonstrates that each has distinct expression patterns, although similarities are observed between clusters III and VI (two of the neuronal modules), and also between the clusters VII and VIII (mixed function and late immune) (Figure 3A). By plotting the relative expression of each gene cluster across time, we could identify four cluster groups with distinct kinetic patterns (Figures 3B–3E). Genes in cluster I (largely chemotaxis related) showed an immediate but short-lived expression change that

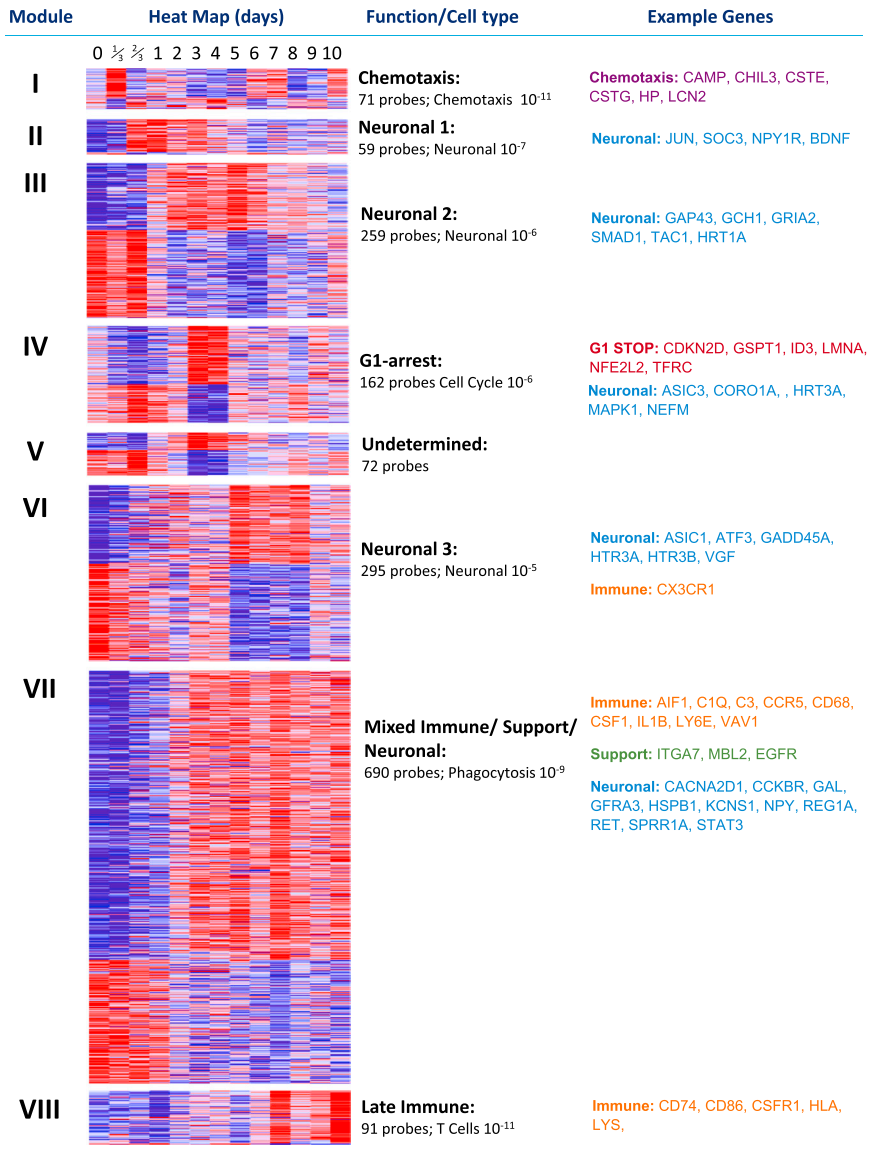

Figure 2. WGCNA Analysis of All Regulated Transcripts in DRG

Significantly regulated probes (moderated F-statistic, n = 1,704) were subject to WGCNA analysis to produce unbiased clusters of co-regulated transcripts representing the entire regulatory network of transcripts in the DRG following peripheral nerve injury (SNI) for 10 days sampled at least once a day over this period. The first column defines the clusters present, and the second shows heatmaps of each gene in each cluster. Blue represents low-level expression and red high-level expression. The third column gives a brief description of cluster function as defined by IPA software. Below this is the number of probes in each cluster and the p value IPA ascribed the function given. The final column gives example transcripts from each functional subdivision. See also Table S1.

peaked several hours post-SNI (Figure 3B). The next kinetic group contained the predominantly neuronal regulatory clusters II, III, and VI, which display a monophasic expression pattern (Figure 3C). Clusters II and III demonstrate a late decrease in relative expression, although average expression did not fall back to baseline by 10 days post-SNI. In contrast, the expression level of cluster VI remained at or around maximal levels until 10 days after SNI. Next, genes in clusters IV and V initially showed a down-regulation in reaction to the injury and then displayed a relatively strong increase that peaked at ~3 days after nerve injury before settling to approximately naive levels at later time points (Figure 3D). The final kinetically distinct group contained two clusters that demonstrated sustained increases of expression, reaching maximal levels over 10 days, with the rise of cluster VII (mixed neuronal/support cell and immune) preceding that of cluster VIII (late immune) (Figure 3E). Each cluster contains not only genes regulated in the direction depicted in Figures 3B–3E but also genes regulated in a pattern mirroring that shown (reciprocal regulation events). Figure 2 shows all gene regulation patterns both positive and negative.

We performed a transcription factor binding site (TFBS) enrichment analysis for each of the eight clusters to uncover the potential regulatory network contributing to the observed gene regulation patterns after nerve injury. To avoid confounders and identify only the most statistically robust sites, we used 3 different control datasets as background (1,000 bp sequences upstream of all mouse genes, mouse CpG islands, and the mouse chromosome 19 sequence). We identified 210 TFs (Figure S1A) whose DNA binding motifs were over represented in the promoters of each gene cluster set (Table S2). Interestingly, hierarchical clustering of the TFBS enrichment score for each cluster revealed a separation of neuronal and immune-associated gene modules, suggesting distinct regulatory control by transcription of these gene sets after nerve injury (Figure S1A).

To identify potential protein signaling pathways operational after nerve injury, we determined the protein-protein interaction (PPI) network represented by all the differentially regulated genes (see Experimental Procedures). We screened for experimentally validated PPI among all possible combinations of gene pairs present in the DRG regulated gene set, obtaining a PPI network consisting of 310 nodes and 442 edges. This revealed certain key signaling molecules such as ATF3, JUN, BDNF, mitogen-activated protein kinase 1/3 (MAPK1/3), transforming growth factor β1 (TGF-β1), STAT3, TCF3, CCR5, and interleukin-1β (IL-1β) (Figure S2) and certain transcription factors (TFs) as major hubs, potentially regulating many of the genes present in the global injury response; including SP1, ESR1,

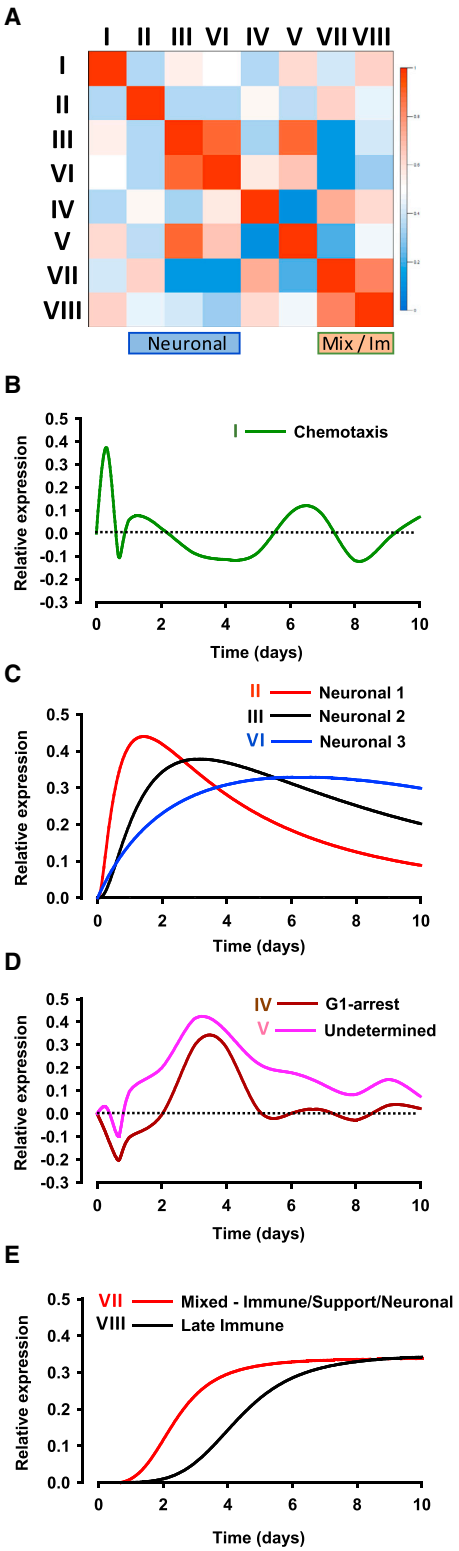

Figure 3. Transcript Regulation in the DRG after SNI Follows Distinct Patterns

(A) Similarity plot of the module eigengenes of each cluster showing very little overlap in pattern regulation.

(B–E) Representations of the regulation of each cluster given as singles line plots with intensity of regulation on the y axis and time on the x axis. Cluster I (B), clusters II, III, and VI (C), clusters IV and V (D), and clusters VII and VIII (E). Each cluster contains not only genes regulated in the fashion drawn but also reciprocal regulation events.

See also Figures S1, S2, and S3 and Tables S1, S2, and S3.

SMAD3, TP53, and STAT5A (Figure S2). Next, by screening for signaling pathways in the PPI network, we observed enrichment of several important signaling pathways that may contribute to nerve injury response, including the neurotrophin, MAPK, TGF-β, chemokine, and ErbB signaling pathways (Table S3). To identify signaling cascades activated over time after nerve injury, we also examined for the presence of signaling pathway genes in each cluster. These analyses show that there is a group of strongly represented neuronal signaling pathways, including NGF, EGFR, p38 MAPK, and TGF-β in clusters III, IV, and VII (Figure S3), suggesting co-activation of multiple signaling pathways in response to nerve injury (Abe and Cavalli, 2008).

Analysis of the full gene expression dataset suggested a generalized kinetic separation of groups of neuronal and immune-rich transcripts across time, such that overall neuronal gene changes preceded alterations in immune transcript expression in the DRG over the first 10 days after nerve damage (Figures 3C and 3E, respectively). This led us to consider whether such expression differences could reveal information on the functional origins of the diverse behavioral manifestations of neuropathic pain.

Genes Correlated with Cold and Tactile Allodynia in the DRG

To define those transcripts with expression changes most correlated with cold and tactile allodynia, we chose transcripts with a Pearson correlation coefficient greater than 0.85 (directly correlated) or less than −0.85 (inversely correlated) with each behavioral hypersensitivity onset curve (Figures 4A and 4B). The cold allodynia time course closely correlated with the temporal pattern of 145 probes, corresponding to 137 distinct transcripts, of which 107 (78%) were upregulated and 30 (22%) were downregulated (Figure 4A). The list of the transcripts correlated with cold allodynia and their Pearson correlation values can be found in Table S4. For tactile allodynia, we identified 40 probes, corresponding to 36 distinct transcripts whose expression closely correlated to the onset of mechanical sensitivity. Of these, 33 transcripts (92%) were upregulated and 3 (8%) were downregulated (Figure 4B). The list of the transcripts correlated with tactile allodynia and their Pearson correlation values can be found in Table S5.

We performed a biological validation of the gene lists that made up the cold- and tactile- correlated groups by comparing these lists with results from DRG transcriptome profiling obtained using RNA sequencing (RNA-seq) (naive and 1, 3, and 7 days after SNI) from biologically distinct tissue to that used in the array studies. We found 116 common genes in the acetone (neuronal) list and 36 common genes in the von Frey (immune) list in both platforms. The heatmaps of common genes from the arrays and RNA-seq for each sensory modality are shown in Figures S2A–S2D, and these data demonstrate that the overall

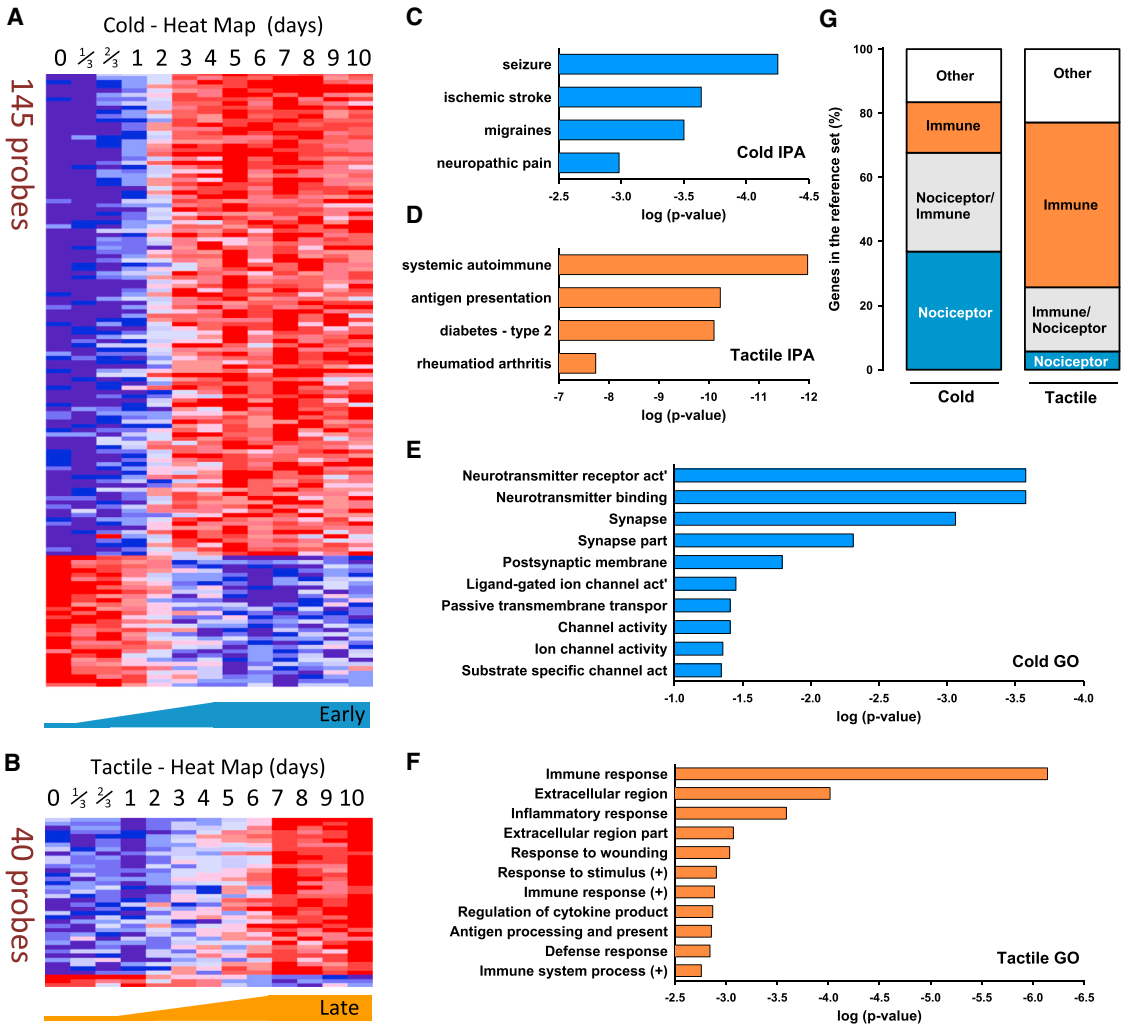

Figure 4. Transcript Expression in the DRG Correlating with the Temporal Profile of Cold Allodynia Was Nociceptor Related, whereas That with Tactile Hypersensitivity Was Immune Cell Centric

Gene expression was correlated with the time courses of cold and tactile allodynia development using the Pearson coefficient of similarity.

(A) Heatmap of the relative expression of the probes that most tightly correlate with cold allodynia onset.

(B) Relative expression of the probes that most tightly correlate with tactile allodynia.

(C and D) Representative functional characteristics using IPA of these cold- (C) and tactile-related (D) transcripts.

(E and F) Strongest GO terms for transcripts correlated with cold (E) and tactile (F) allodynia.

(G) Cross-comparison of transcripts present in each cluster with transcript lists derived from isolated DRG nociceptors and isolated macrophages/T cells. Orange represents genes contained only in the immune gene list, blue represents genes contained only in the nociceptor list, gray represents genes present in both lists, and white represents genes not contained in either list.

See also Tables S4, S5, S6, S7, S8, and S9 and Figure S4.

expression patterns of the constituent genes were virtually identical regardless of the platform used to define gene regulation. This RNA-seq dataset also allows validation of the other regulated transcripts described in Figure 2.

When the group of genes correlated with cold allodynia was processed by IPA, "Neurological disease" was the top biological function defined for 33 genes (24%). "Seizures," "Migraines," and "Neuropathic pain" were also among functional subgroups identified as present (Figure 4C). (See Table S6 for the content of genes in each annotated function.) In contrast, for the group of genes significantly correlated with tactile allodynia, with IPA, "Immune disease" was identified as the top biological function, with 19 transcripts (53%). "Systemic autoimmune syndrome," "Antigen presentation activation," "Insulin-dependent diabetes mellitus," and "Rheumatoid arthritis" were other functional subgroups identified as present (Figure 4D). (See Table S7 for the content of genes in each annotated function.)

To further assay genes associated with the development of cold and tactile allodynia, we investigated a more inclusive group of transcripts including those genes directly and inversely correlated with a Pearson coefficient of correlation >0.75 (see Experimental Procedures). These gene sets were then subjected to

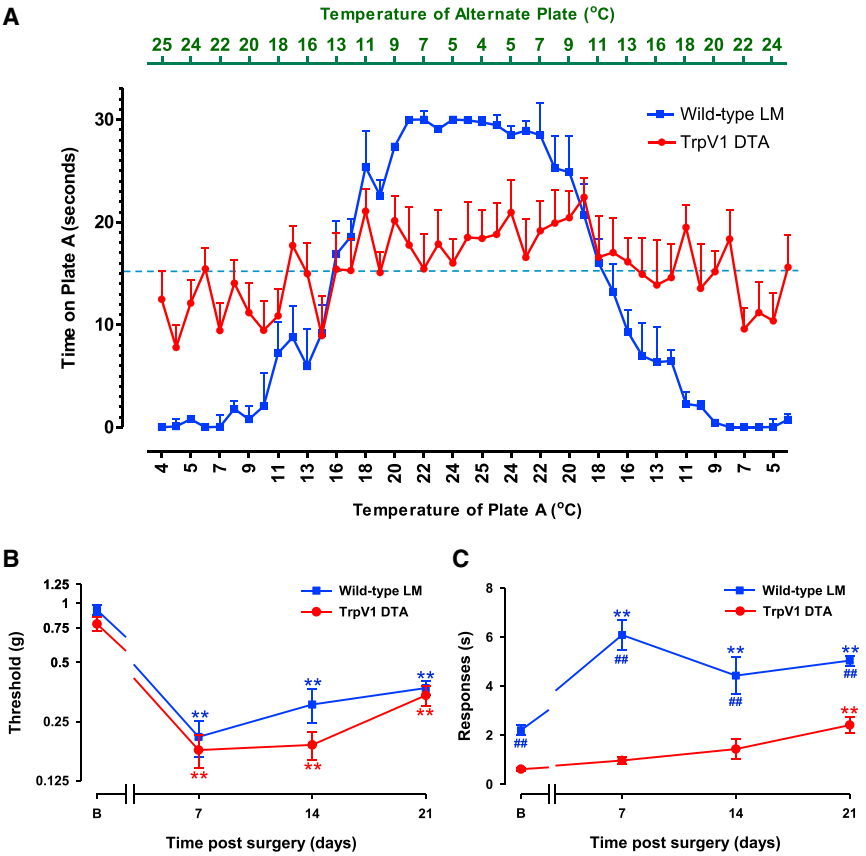

Figure 5. Trpv1 Lineage Neuronal Deletion Mice Develop Tactile, but Not Cold, Allodynia after SNI Injury

(A) When naive mice are given the choice between two opposing temperatures, wild-type control littermate (LM) mice move toward the more ambient temperature, whereas Trpv1 DTA mice do not. Each point on the graph measures the amount of time spent on plate A in a 30-s window (y axis) when the plate was set to the temperature given on the lower x axis. The top x axis gives the temperature of the alternate plate for that time bin.

(B) TrpV1 lineage DTA mice and their LM control counterparts develop tactile allodynia post-SNI. Statistically significant differences between the values from mice after SNI and their basal measures are shown (**$p < 0.01$). However, there was no significant difference between the two curves (two-way repeated-measures ANOVA).

(C) TrpV1 lineage DTA mice develop very weak levels of cold allodynia relative to their LM controls. Statistically significant differences between the values from mice after SNI and their basal measures (**$p < 0.01$) and between wild-type LM controls and TrpV1 DTA mice in cold sensitivity (##$p < 0.01$) are shown (two-way repeated-measures ANOVA, Bonferroni post hoc test).

For (A), n = 9 (TrpV1-DTA), n = 10 (LM controls); for (B) and (C), n = 8 (both groups). Error bars indicate SEM. See also Figure S5.

Gene Ontology (GO) analysis to find the most related functional terms (Figures 4E and 4F). Transcripts in this set whose expression over time correlated with the onset of cold allodynia (375 probes) were almost entirely related to neuronal function (Figure 4E). (See Table S8 for the content of genes in each annotated function.) The genes most related to the development of tactile allodynia in the GO analysis were almost entirely related to immune function (130 probes). (See Table S9 for the content of genes in each annotated function.) Both GO analyses accord with the IPA-based data (shown in Figures 4E and 4F).

An enrichment of a particular IPA functional annotation or GO category signifies that multiple genes participating in the same process correlate with the phenotype in question. Using two thresholds of correlation allowed us to span the expression data more exhaustively than using one. The fact that each of these lists result in very complementary functional descriptions using two different pathway search tools with different correlated transcript inclusion criteria represents an internal control for the validity of the associations.

We also compared the cold- and tactile-allodynia-correlated transcripts to previously published analyses of genes specifically expressed either in nociceptor DRG neurons (Chiu et al., 2014) or in activated macrophages and T cells (Brown et al., 2015; Rosas et al., 2014) (see Experimental Procedures). This analysis revealed that 37% of the genes identified as correlated with cold allodynia are expressed specifically in nociceptors, with 16% specific to leukocytes. Using the same approach to assay genes whose expression correlates with tactile allodynia, 51% are specifically expressed in leukocytes, with only 6% specific to nociceptors. Therefore, transcripts correlated with the onset of tactile allodynia have a stronger immune component than neuronal, with the reverse holding true for cold allodynia (Figure 4G).

TrpV1 Lineage Neurons and Neuropathic Allodynia

To determine if changes in a specific set of DRG sensory neurons are responsible for development of cold allodynia post-SNI, we examined *TrpV1^{Cre}DTA$^{flox\text{-}stop}$* mice that lack TrpV1-lineage nociceptors but retain mechanoreceptors (Mishra et al., 2011). We first assessed cold sensitivity in naive (uninjured) *TrpV1^{Cre}DTA$^{flox\text{-}stop}$* mice and their wild-type littermates in a dynamic thermal place cold aversion challenge. While the littermate control mice rapidly manifested a preference for moderate (11°C–25°C) rather than noxious cold (4°C–11°C) temperatures, *TrpV1^{Cre}DTA$^{flox\text{-}stop}$* mice displayed no aversion to noxious cold. These data indicate that TrpV1 lineage nociceptors are essential for cold detection under baseline conditions (Figure 5A).

Next, we determined the temporal development of tactile and cold allodynia after SNI in the TrpV1 neuron ablated mice relative to their littermate controls. TrpV1 DTA mice showed a total loss of TrpV1 expression in the DRG (Figure S5A), indicating the efficiency of the ablation. The tactile behavioral hypersensitivity was fully apparent in these mice at 7 days post-SNI injury and continued at similar levels until at least 21 days post-SNI

(Figure 5B). In contrast, TrpV1 DTA mice failed to develop cold allodynia 7 or 14 days after nerve injury (Figure 5C). The lack of normal cold- or injury-induced cold sensitivity in these animals may reflect the absence of TrpM8 expression in the DRG relative to wild-type controls (Figure S5B). At later time points (21 days), injured TrpV1 DTA mice developed a slight level of cold allodynia relative to naive TrpV1 DTA mice (Figure 5C). The mechanism for this late and muted response is unclear, although it likely represents compensatory changes in gene expression/function in the remaining (non TRPV1 lineage) intact sensory neurons that enable them to develop sufficient cold thermoception to drive the central circuits that produce cold allodynia. Some residual TrpA1 (but not TrpM8) expression is present in the DRGs of TrpV1 DTA mice (~20% of wild-type levels) (Figure S5C), and TrpA1 is implicated in neuropathic cold allodynia (del Camino et al., 2010), suggesting this channel maybe the source of this late-onset low-level activity. The early loss in cold allodynia in TrpV1 DTA mice is consistent with the primarily neuronal gene expression changes in the DRG that correlate with its onset. Based on these findings, we conclude that an alteration in TrpV1 lineage sensory neurons is required for early development of this phenotype.

Peripheral Macrophages Are Crucial to the Development of Tactile, but Not Cold, Allodynia

Genes whose expression pattern matched the time course of tactile allodynia onset are primarily expressed in immune cells. Specifically, they appear to be enriched in macrophages and T cells (Figure 4G), two leukocyte populations present in DRGs after nerve injury (Hu and McLachlan, 2002; Moalem and Tracey, 2006) (see also Figures 7A and 7B). To assess whether circulating macrophages have a role in mediating allodynia, we transiently depleted them in C57BL/6 mice using liposomal clodronate. Macrophages naturally phagocytose these liposomes within the blood; this releases clodronate intracellularly and results in their death. Following a single liposomal clodronate dose, animals regenerate a full macrophage blood count from bone marrow precursors over the next 2 weeks (Camilleri et al., 1995). Animals administered with liposomal clodronate 1 day before nerve injury (SNI) developed minimal tactile allodynia at 7 and 10 days post-SNI relative to control mice treated with empty liposomes (Figure 6A). However, clodronate-treated and control animals developed cold allodynia to a similar extent post-SNI (Figure 6B). By assaying the blood at 7 days post-SNI, we found markedly reduced myeloid cells in clodronate-treated mice relative to liposome controls (Figure 6C). These changes also translated to the DRG tissue (Figures 6D and 6E), which may explain the large differences in mechanical threshold in the same mice (Figure 6F). We confirmed the decrease in macrophages/monocytes by immunohistochemistry; liposome control mice showed a marked IBA1 immunoreactivity in the ipsilateral L3-5 DRGs 7 days post-SNI, and this was markedly decreased in clodronate-treated mice (Figures 6G and 6H, respectively). We further quantified the relative expression within the injured DRG by qPCR of the macrophage/monocyte markers CD68 and CD11b, which both showed significant decreases relative to liposome control mice (Figures 6I and 6J, respectively). In addition, we quantified the transcript of CD163 (a marker of tissue resident macrophages), which was strongly decreased following clodronate treatment (Figure 6K).

Consequence of Absence of T and B Cells on Nerve-Injury-Induced Tactile and Cold Hypersensitivity

To demonstrate whether in addition to macrophages, activated T cells were also present in the ipsilateral DRG 7 days post-SNI injury, we utilized a combination of a Lck-zsGreen mouse line, which expresses the fluorescent marker zsGreen in activated T cells (Zhang et al., 2005), and immunostaining for IBA1. In the uninjured Lck-zsGreen transgenic DRG, very few labeled T cells were present and there was little IBA1 staining (Figure 7A). In ipsilateral DRGs 7 days post-SNI, there were in contrast many labeled T cells and a strong IBA1 signal (red, Figure 7B). To test whether the absence of T cells had any effect on cold and tactile allodynia, we exploited *Rag1*$^{-/-}$ mice that lack T and B cells (Figure 7C, left and middle). In agreement with our previous observations (Costigan et al., 2009a), we found a marked reduction in tactile hypersensitivity in *Rag1*$^{-/-}$ animals relative to their littermate controls (Figure 7D). We extended this by showing that introducing CD4^{+}/CD8^{+} T cells into *Rag1*$^{-/-}$ mice (Figure 7C) could rescue the tactile allodynia phenotype for at least 4 weeks post-SNI (Figure 7D). The full rescue of tactile allodynia by T cells in reconstituted *Rag1*$^{-/-}$ mice, which still lack B cells, argues against a role for this latter immune cell type in this phenotype (Figures 7C and 7D). In contrast, we witnessed little difference in the extent of cold allodynia in *Rag1*$^{-/-}$ animals (Figure 7E), suggesting that both T and B cells are dispensable for that response.

Taken together, these data strongly support a role for of each of these two leukocyte cell types (macrophages and T cells) in the establishment of tactile allodynia after peripheral nerve damage but demonstrate that they are dispensable for the development of cold allodynia.

DISCUSSION

By assaying the development of two common clinical manifestations of stimulus-evoked neuropathic pain (cold and tactile allodynia) (Jensen and Finnerup, 2014) at high temporal resolution, we demonstrate that they develop over different time courses in the first week post-surgery in the SNI model. This difference led us to hypothesize that there may be mechanistic differences underlying these two pain modalities and that these could perhaps be revealed by correlating the changes in global transcript expression in the PNS in response to nerve injury with the temporal evolution of the behavior. To investigate this, we generated DRG expression array profiles beginning immediately after the nerve injury and at a higher temporal definition than in previous investigations (Costigan et al., 2010; Li et al., 2015).

To assay global transcript expression changes in the DRG following SNI, we separated all of the potentially regulated genes into co-regulated clusters using WGCNA, since groups of genes with similar expression patterns across large datasets are often functionally connected as part of the same tissue, cell type, or biological pathway (Parikshak et al., 2015). There were relatively few clustered groups of co-regulated transcripts in the injured DRG over the 10 days following the injury (eight in total), with a

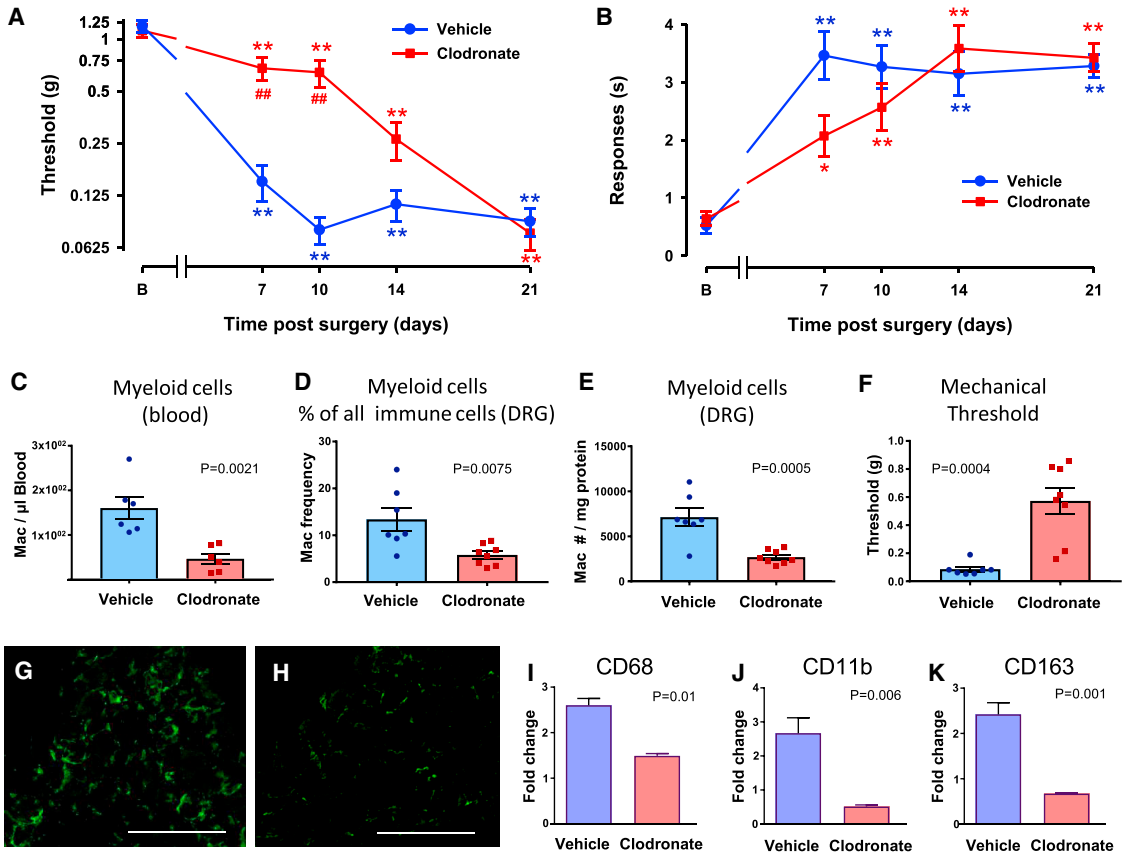

Figure 6. Mice Depleted of Peripheral Macrophages/Monocytes Using Clodronate Develop Delayed Tactile Allodynia but Normal Neuropathic Cold Allodynia

(A) Clodronate-treated mice develop markedly less tactile allodynia post-peripheral nerve injury than empty-liposome-treated controls.

(B) Clodronate-treated mice develop significant levels of cold allodynia post-SNI. Statistically significant differences between the values from mice after SNI and their basal measure (**$p < 0.01$) and between mice treated with clodronate or vehicle in tactile allodynia (##$p < 0.01$) are shown (two-way repeated-measures ANOVA, Bonferroni post hoc test). Clodronate-treated C57BL/6 mice develop significant levels of cold allodynia post-SNI (*$p < 0.05$, **$p < 0.01$), but there were no significant differences in cold allodynia between clodronate- and vehicle-treated mice ($p = 0.323$; two-way repeated-measures ANOVA).

For (A) and (B), n = 10 clodronate, n = 13 vehicle.

(C–E) Levels of myelocytes ($CD45^+CD11b^+CD11c^-SiglecF^-CD3^-$) measured by FACS in blood (C) and DRG (D and E) 7 days after SNI in mice treated with clodronate or vehicle.

(F) Mechanical threshold in these mice.

For (C)–(F), p values are given (unpaired Student's t test).

(G and H) Iba1 immunoreactivity in the DRG from SNI mice treated with vehicle liposomes (G) or clodronate liposomes (H). Scale Bar: 100 µm.

(I–K) Real-time qPCR of the macrophage/monocyte markers CD68 (I), CD11b (J), and CD163 (K) in the DRG of SNI mice treated with liposomes or clodronate. p values are given (n = 5 per group; unpaired Student's t test).

Error bars indicate SEM.

temporal analysis suggesting an early pattern of neuronal gene regulation followed later by regulation of immune transcripts. Correlation of the distinct trajectories of cold and tactile hypersensitivity onset respectively with gene expression further suggested a link between the two. The patterns suggest predominant involvement of sensory neurons in the onset of cold allodynia and a contribution of activated peripheral immune cells in the generation of tactile allodynia. Next, we used a combination of genetically targeted and cell depletion protocols to test these predictions.

TrpV1-mediated Cre expression in the embryo occurs in all thermo-sensing progenitor neurons, which are consequently deleted by DTA expression. This removes all TrpM8 expression and, therefore, all normo-cold sensation in the adult mouse, as shown here and in previous studies (McKemy, 2011; Mishra et al., 2011). We demonstrate that ablating TrpV1 lineage nociceptors results in a lack of cold allodynia after nerve injury, consistent with this process occurring primarily through neuronal mechanisms. In addition, recent independent data are entirely consistent with cold allodynia occurring through neuronal signaling pathways (Lippoldt et al., 2016).

Cold allodynia, like tactile allodynia following SNI, must be the consequence of input to the CNS transmitted by uninjured sural nerve axons. This raises the question of whether something

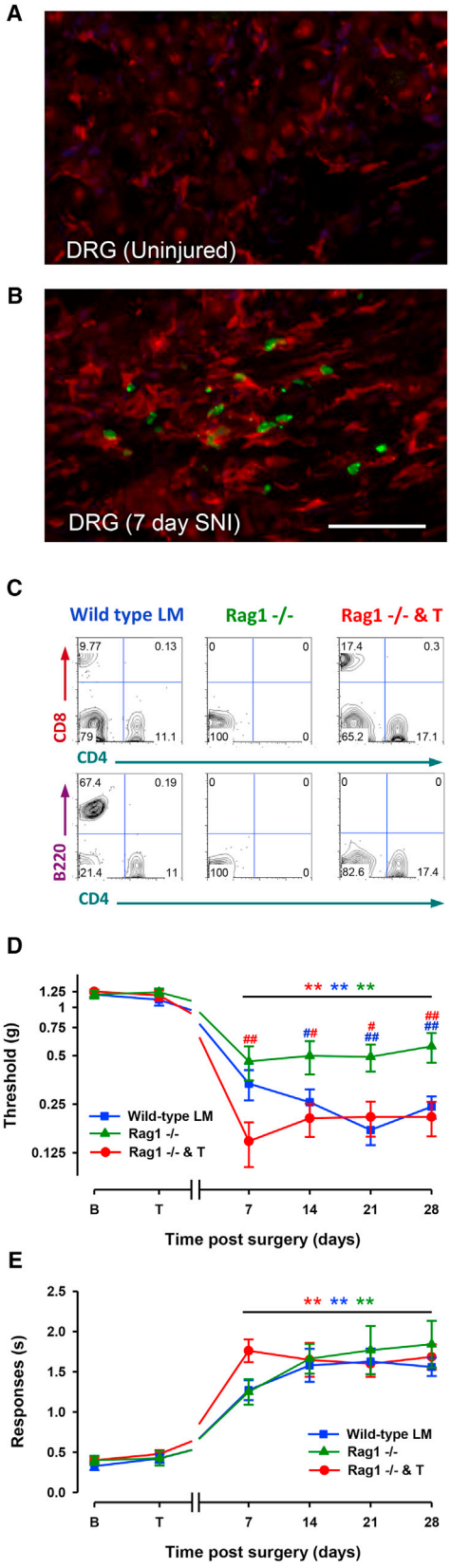

Figure 7. T and B Cell-Deficient *Rag1*$^{-/-}$ Mice Develop Normal Neuropathic Cold Allodynia, but Not Complete Tactile Allodynia, following SNI Injury

T cell reintroduction into *Rag1*$^{-/-}$ mice abolishes tactile sensitivity differences present between *Rag1*$^{-/-}$ mice and wild-type control littermates (LM) but leaves cold allodynia unaltered.

(A and B) Immunohistochemistry for the monocyte/macrophage marker IBA1 (red) in noninjured (A) and 7-day SNI-injured DRG in Lck Cre-zsGreen mice, which express labeled T cells (green) (B). Scale Bar: 50 μm.

(C) Representative FACS plots of CD4 versus CD8 cell counts from splenic preparation showing cells positive for both markers in the wild-type and in *Rag1*$^{-/-}$ and T mice, but not *Rag1*$^{-/-}$ mice (top). Representative FACS plots of CD4 versus B220 counts showing the presence of B cells in wild-type LMs, but not *Rag1*$^{-/-}$ or reconstituted *Rag1*$^{-/-}$ mice.

(D) *Rag1*$^{-/-}$ mice develop less tactile allodynia post-SNI than their LM controls (Rag versus WT, $p = 0.003$; Rag versus Rag and T, $p = 0.002$). Reconstituted *Rag1*$^{-/-}$ mice (*Rag1*$^{-/-}$ and T) showed full levels of tactile sensitivity (WT versus Rag and T, not significantly different). Significant differences between the values after SNI and their basal measures are shown (**$p < 0.01$, *Rag1*$^{-/-}$ mice versus WT littermates [blue #]; *Rag1*$^{-/-}$ mice versus Rag and T [red #]; #$p < 0.05$, ##$p < 0.01$, two-way repeated-measures ANOVA, Bonferroni post hoc test).

(E) Wild-type LMs, *Rag1*$^{-/-}$, and T cell-reconstituted mice develop similar neuropathic cold allodynia (no significant differences among the three curves). For (D) and (E), error bars indicate SEM (wild-type LM, n = 15; *Rag1*$^{-/-}$, n = 10; *Rag1*$^{-/-}$ and T, n = 15).

changes in these "uninjured" peripheral neurons due to the SNI procedure, such that previously innocuous stimuli can now activate a set of nociceptors or if there is an abnormal reaction in the CNS, such that the 'normal input' generated by innocuous temperatures in spared fibers now elicits pain-like behavior? For the former, one might speculate that injured sensory neurons may produce paracrine signals in the DRG that somehow alter the sensitivity of neighboring non-injured thermo-nociceptors to cold. For the latter, as injured C-nociceptors become ectopically active early following peripheral nerve injury (4–13 hr) (Kirillova et al., 2011), this abnormal afferent drive could maintain central sensitization altering the central processing of low-threshold thermoceptor inputs in the dorsal horn, leading to them being perceived as painful (Latremoliere and Woolf, 2009).

In spite of the marked reduction in cold allodynia seen in the TrpV1 DTA line, we found relatively normal levels of tactile allodynia in these mice, which rules out the specific need for this nociceptor lineage in the production of this form of stimulus-evoked pain hypersensitivity after nerve injury. These findings are in agreement with previous reports showing that ablation of either TrpV1 or Nav1.8 lineage nociceptor neurons does not alter neuropathic tactile allodynia (Abrahamsen et al., 2008; Lagerström et al., 2011; Mishra et al., 2011). Tactile allodynia must require other sensory neurons for its manifestation, and indeed many studies have indicated that it is carried by low-threshold mechanoreceptors (Campbell and Meyer, 2006; Xu et al., 2015).

The correlation of immune related transcripts with the development of tactile allodynia suggested that the immune system may play a role in the development of this hypersensitivity, but that these cells are largely dispensable for cold allodynia. To test this prediction, we targeted two leukocyte populations, macrophages/monocytes and T cells, as these cells represent a large portion of the immune reaction within the DRG following nerve injury (Hu and McLachlan, 2002; Moalem and Tracey,

2006), and found that both peripheral macrophages and T cells contribute to the development of neuropathic tactile sensitivity but minimally to cold allodynia.

T cells and macrophages play a major role in orchestrating the actions of one another during the early and late phases of the immune response (Biswas et al., 2012; Roberts et al., 2015). The complex interplay between innate and adaptive components of the immune system is a major component of the reaction of the PNS to damage, with functional roles in clearance of debris and promotion of regeneration (DeFrancesco-Lisowitz et al., 2015). However, recruitment of these leukocytes following nerve injury can lead to effects on sensory neurons that activate or sensitize them, leading to neuropathic pain (Costigan et al., 2009b).

Following nerve injury, macrophage-derived signaling molecules such as IL-1β, TNF-α, and CCL2 likely contribute to pain-like hypersensitivity (Andrade et al., 2014; Schuh et al., 2014; Zhu et al., 2014) as well as the initiation of axonal regrowth (Dubový et al., 2013). In turn, Th1 T cell-derived interferon-γ (IFN-γ) can recruit macrophages to sites of inflammation and cause pain (Liou et al., 2011), whereas type 2 inflammatory cytokines, such as IL-4, IL-10, and TGF-β, can ameliorate neuropathic pain-like behavior (Chen et al., 2015; Dengler et al., 2014; Kiguchi et al., 2015). The balance between these pro- and anti-inflammatory subsets in different experimental settings may explain the differences seen between studies focused on the role of T cells on neuropathic pain (Austin et al., 2012; Kiguchi et al., 2015); some studies did not find any impact on the pain phenotype of T cell actions (Sorge et al., 2015), whereas we and several others have (Cao and DeLeo, 2008; Costigan et al., 2009a; Kobayashi et al., 2015; Leger et al., 2011; Zhang et al., 2014).

While the mechanisms by which macrophages and T cells interact to co-produce a convergent set of changes in the DRG that lead to tactile allodynia now need to be explored, our data indicate that they must act on sensory fibers other than TrpV1 lineage nociceptors. Activated macrophages are seen preferentially around injured large-diameter A-fiber sensory neuron cell bodies in the DRG after sciatic nerve injury (Vega-Avelaira et al., 2009), but the functional consequence of this on these sensory neurons is still unknown. It is possible that activated immune cells in the DRG may stimulate injured A-fibers into initiating ectopic activity, which contributes to the maintenance of central sensitization in the dorsal horn, such that central pain neurons begin to be activated by low-threshold mechanoreceptors. In the naive state, only C-fibers can initiate central sensitization, but after nerve injury, A-fibers develop this capacity by a phenotypic switch (Decosterd et al., 2002), and this shift may be triggered by immune cell activation in the DRG. Consistent with this, ectopic firing of injured A-fiber neurons manifests later after nerve injury than in C-fibers (ectopic A-fiber activity is seen at 4–7 days) (Kirillova et al., 2011). Alternatively, spared high-threshold A-fiber nociceptors may be sensitized by immune cell action following peripheral nerve damage. Either of these mechanisms, or possibly a combination of both, may lead to mechanical allodynia. What we now show conclusively, however, is that the mechanism responsible is dependent on peripheral immune cells.

Distinct mechanistic etiologies for these two neuropathic pain symptoms may in consequence require different treatment strategies, if our findings translate to humans, one targeted at a particular set of TRPV1 lineage nociceptors for patients whose primary symptoms are cold allodynia and another for patients with predominant tactile allodynia, which could incorporate either targeting the actions of the immune component of nerve injury (macrophages and/or T cells) or non-TRPV1-expressing afferents (mechanoreceptors). Identifying the key elements of immune-neural signaling that underlie the development of allodynia after nerve damage using cell-specific profiling technologies will be important for developing targeted therapies for peripheral neuropathic pain.

EXPERIMENTAL PROCEDURES

Experiments were performed in adult (9–10 weeks old) male C57BL/6J mice (Jackson Laboratory [Jax], ME). Heterozygous TrpV1-Cre (strain 017769) and heterozygous DTA stop animals (strain 010527) were bred together to produce TrpV1 DTA animals. Rag1 null (strain 2216) mice were also used. To reveal T cell infiltration in the injured DRG, we bred Lck-Cre (Jackson Laboratory [Jax] 3802) mice with zsGreen reporter mice (Rosa-CAG-LSL-ZsGreen1-WPRE) (Jax 7906). All studies performed in USA were reviewed and approved by the IACUC at Boston Children's Hospital under animal protocols 15-04-2928R and 16-01-3080R. All experimental procedures performed in Spain were conducted in strict accordance to European standards (European Communities Council Directive 2010/63) and after approval of the animal protocols by regional (Junta de Andalucía) and institutional (Research Ethics Committee of the University of Granada, Spain) authorities.

Detailed description of the animal strains used and the experimental procedures for surgeries (SNI), behavioral tests (von Frey test, acetone test and dynamic thermal place aversion test), immune cell depletion or reconstitution, gene expression analysis by microarray, RNA-seq and real-time qPCR, bioinformatics (weighted gene co-expression network analysis, correlation between expression changes and the pain phenotype, functional enrichment analysis, transcription-factor-binding site enrichment, and PPI network analyses); fluorescence-activated cell sorting to determine myeloid cells or T and B cells, and immunohistochemistry are described in Supplemental Experimental Procedures.

Statistical Significance

Gene regulation in the expression microarrays was determined by a moderated F-statistics using Bioconductor packages. In the rest of the experiments, multiple comparisons were analyzed using repeated-measures ANOVA with Bonferroni post-test, and single comparisons were analyzed using an unpaired Student's t test. Statistical analyses were performed with SigmaPlot 12.0 software (Systat Software, CA), with significance defined as $p < 0.05$.

DATA AND SOFTWARE AVAILABILITY

The accession number for all microarray and RNA-seq datasets reported in this paper is GEO: GSE102937.

SUPPLEMENTAL INFORMATION

Supplemental Information includes Supplemental Experimental Procedures, five figures, and nine tables and can be found with this article online at https://doi.org/10.1016/j.celrep.2018.01.006.

ACKNOWLEDGMENTS

This study was supported by NIH grants R01NS074430 (M.C.), R01NS58870, and R37NS039518 (C.J.W.); the Dr. Miriam and Sheldon G. Adelson Medical Research Foundation (C.J.W., G.C., and D.G.); NINDS Informatics Center for Neurogenetics and Neurogenomics (P30 NS062691) (F.G. and G.C.); Neurodevelopmental Behavior Core, grant CHB IDDRC, 1U54HD090255 (N.A.A.);

and grants SAF2013-47481P and SAF2016-80540-R from the Spanish Ministry of Economy and Competitiveness (MINECO) and the European Regional Development Fund (FEDER) (E.J. Cobos). E.J. Cobos was supported by the Research Program of the University of Granada. I.B.-C. was supported by an FPU grant from MINECO. R.G.C. was supported by the Alfonso Martin Escudero fellowship. F.R.N. was supported by a Juan de la Cierva postdoctoral grant from MINECO. M.R. was supported by a Junior-1 salary support award from the Fonds de recherche du Québec - Santé (FRQS).

AUTHOR CONTRIBUTIONS

Conceptualization, M.C. and C.J.W.; Methodology, M.C., C.J.W., E.J. Cobos, and E.J. Chesler; Formal Analysis, E.J. Cobos, C.A.N., F.G., V.C., M.W.P., D.H.G., G.C., M.R., C.J.W., and M.C.; Investigation, E.J. Cobos, C.A.N., I.B.-C., R.G.-C., N.A.A., A.L., C.R.S., G.P., F.R.N., N.J., M.W.P., P.R., M.R., and M.C.; Resources, G.C. and D.H.G.; Data Curation, E.J. Cobos, G.C., F.G., D.H.G., and M.C.; Writing – Original Draft, M.C., E.J. Cobos, and C.J.W.; Writing – Review & Editing, E.J. Cobos, C.A.N., F.G., V.C., I.B.-C., R.G.-C., P.R., N.A.A., A.L., C.R.S., G.P., F.R.N., N.J., M.W.P., C.H.E.M., T.O., E.J. Chesler, D.H.G., G.C., M.R., C.J.W., and M.C.; Visualization, E.J. Cobos, I.B.-C., A.L., V.C., and M.C., Supervision, M.C., G.C., and C.J.W.; Project Administration, E.J. Cobos, G.C., M.C., and C.J.W.; Funding Acquisition, E.J. Cobos, M.C., and C.J.W.

DECLARATION OF INTERESTS

The authors declare no competing interests.

Received: February 17, 2017
Revised: August 23, 2017
Accepted: January 2, 2018
Published: January 30, 2018

REFERENCES

Abe, N., and Cavalli, V. (2008). Nerve injury signaling. Curr. Opin. Neurobiol. *18*, 276–283.

Abrahamsen, B., Zhao, J., Asante, C.O., Cendan, C.M., Marsh, S., Martinez-Barbera, J.P., Nassar, M.A., Dickenson, A.H., and Wood, J.N. (2008). The cell and molecular basis of mechanical, cold, and inflammatory pain. Science *321*, 702–705.

Andrade, P., Hoogland, G., Del Rosario, J.S., Steinbusch, H.W., Visser-Vandewalle, V., and Daemen, M.A. (2014). Tumor necrosis factor-α inhibitors alleviation of experimentally induced neuropathic pain is associated with modulation of TNF receptor expression. J. Neurosci. Res. *92*, 1490–1498.

Austin, P.J., Kim, C.F., Perera, C.J., and Moalem-Taylor, G. (2012). Regulatory T cells attenuate neuropathic pain following peripheral nerve injury and experimental autoimmune neuritis. Pain *153*, 1916–1931.

Biswas, S.K., Chittezhath, M., Shalova, I.N., and Lim, J.Y. (2012). Macrophage polarization and plasticity in health and disease. Immunol. Res. *53*, 11–24.

Brown, C.C., Esterhazy, D., Sarde, A., London, M., Pullabhatla, V., Osma-Garcia, I., Al-Bader, R., Ortiz, C., Elgueta, R., Arno, M., et al. (2015). Retinoic acid is essential for Th1 cell lineage stability and prevents transition to a Th17 cell program. Immunity *42*, 499–511.

Camilleri, J.P., Williams, A.S., Amos, N., Douglas-Jones, A.G., Love, W.G., and Williams, B.D. (1995). The effect of free and liposome-encapsulated clodronate on the hepatic mononuclear phagocyte system in the rat. Clin. Exp. Immunol. *99*, 269–275.

Campbell, J.N., and Meyer, R.A. (2006). Mechanisms of neuropathic pain. Neuron *52*, 77–92.

Cao, L., and DeLeo, J.A. (2008). CNS-infiltrating CD4+ T lymphocytes contribute to murine spinal nerve transection-induced neuropathic pain. Eur. J. Immunol. *38*, 448–458.

Chen, G., Park, C.K., Xie, R.G., and Ji, R.R. (2015). Intrathecal bone marrow stromal cells inhibit neuropathic pain via TGF-β secretion. J. Clin. Invest. *125*, 3226–3240.

Chiu, I.M., Barrett, L.B., Williams, E.K., Strochlic, D.E., Lee, S., Weyer, A.D., Lou, S., Bryman, G.S., Roberson, D.P., Ghasemlou, N., et al. (2014). Transcriptional profiling at whole population and single cell levels reveals somatosensory neuron molecular diversity. eLife *3*, e04660.

Colleoni, M., and Sacerdote, P. (2010). Murine models of human neuropathic pain. Biochim. Biophys. Acta *1802*, 924–933.

Costigan, M., Befort, K., Karchewski, L., Griffin, R.S., D'Urso, D., Allchorne, A., Sitarski, J., Mannion, J.W., Pratt, R.E., and Woolf, C.J. (2002). Replicate high-density rat genome oligonucleotide microarrays reveal hundreds of regulated genes in the dorsal root ganglion after peripheral nerve injury. BMC Neurosci. *3*, 16.

Costigan, M., Moss, A., Latremoliere, A., Johnston, C., Verma-Gandhu, M., Herbert, T.A., Barrett, L., Brenner, G.J., Vardeh, D., Woolf, C.J., and Fitzgerald, M. (2009a). T-cell infiltration and signaling in the adult dorsal spinal cord is a major contributor to neuropathic pain-like hypersensitivity. J. Neurosci. *29*, 14415–14422.

Costigan, M., Scholz, J., and Woolf, C.J. (2009b). Neuropathic pain: a maladaptive response of the nervous system to damage. Annu. Rev. Neurosci. *32*, 1–32.

Costigan, M., Belfer, I., Griffin, R.S., Dai, F., Barrett, L.B., Coppola, G., Wu, T., Kiselycznyk, C., Poddar, M., Lu, Y., et al. (2010). Multiple chronic pain states are associated with a common amino acid-changing allele in KCNS1. Brain *133*, 2519–2527.

Decosterd, I., and Woolf, C.J. (2000). Spared nerve injury: an animal model of persistent peripheral neuropathic pain. Pain *87*, 149–158.

Decosterd, I., Allchorne, A., and Woolf, C.J. (2002). Progressive tactile hypersensitivity after a peripheral nerve crush: non-noxious mechanical stimulus-induced neuropathic pain. Pain *100*, 155–162.

DeFrancesco-Lisowitz, A., Lindborg, J.A., Niemi, J.P., and Zigmond, R.E. (2015). The neuroimmunology of degeneration and regeneration in the peripheral nervous system. Neuroscience *302*, 174–203.

del Camino, D., Murphy, S., Heiry, M., Barrett, L.B., Earley, T.J., Cook, C.A., Petrus, M.J., Zhao, M., D'Amours, M., Deering, N., et al. (2010). TRPA1 contributes to cold hypersensitivity. J. Neurosci. *30*, 15165–15174.

Dengler, E.C., Alberti, L.A., Bowman, B.N., Kerwin, A.A., Wilkerson, J.L., Moezzi, D.R., Limanovich, E., Wallace, J.A., and Milligan, E.D. (2014). Improvement of spinal non-viral IL-10 gene delivery by D-mannose as a transgene adjuvant to control chronic neuropathic pain. J. Neuroinflammation *11*, 92.

Dib-Hajj, S.D., and Waxman, S.G. (2014). Translational pain research: Lessons from genetics and genomics. Sci. Transl. Med. *6*, 249sr4.

Dubový, P., Jančálek, R., and Kubek, T. (2013). Role of inflammation and cytokines in peripheral nerve regeneration. Int. Rev. Neurobiol. *108*, 173–206.

Hu, P., and McLachlan, E.M. (2002). Macrophage and lymphocyte invasion of dorsal root ganglia after peripheral nerve lesions in the rat. Neuroscience *112*, 23–38.

Hu, P., Bembrick, A.L., Keay, K.A., and McLachlan, E.M. (2007). Immune cell involvement in dorsal root ganglia and spinal cord after chronic constriction or transection of the rat sciatic nerve. Brain Behav. Immun. *21*, 599–616.

Jaggi, A.S., Jain, V., and Singh, N. (2011). Animal models of neuropathic pain. Fundam. Clin. Pharmacol. *25*, 1–28.

Jensen, T.S., and Finnerup, N.B. (2014). Allodynia and hyperalgesia in neuropathic pain: clinical manifestations and mechanisms. Lancet Neurol. *13*, 924–935.

Kiguchi, N., Kobayashi, Y., Saika, F., Sakaguchi, H., Maeda, T., and Kishioka, S. (2015). Peripheral interleukin-4 ameliorates inflammatory macrophage-dependent neuropathic pain. Pain *156*, 684–693.

Kirillova, I., Rausch, V.H., Tode, J., Baron, R., and Jänig, W. (2011). Mechano- and thermosensitivity of injured muscle afferents. J. Neurophysiol. *105*, 2058–2073.

Kobayashi, Y., Kiguchi, N., Fukazawa, Y., Saika, F., Maeda, T., and Kishioka, S. (2015). Macrophage-T cell interactions mediate neuropathic pain through the glucocorticoid-induced tumor necrosis factor ligand system. J. Biol. Chem. *290*, 12603–12613.

LaCroix-Fralish, M.L., Austin, J.S., Zheng, F.Y., Levitin, D.J., and Mogil, J.S. (2011). Patterns of pain: meta-analysis of microarray studies of pain. Pain *152*, 1888–1898.

Lagerström, M.C., Rogoz, K., Abrahamsen, B., Lind, A.L., Olund, C., Smith, C., Mendez, J.A., Wallén-Mackenzie, Å., Wood, J.N., and Kullander, K. (2011). A sensory subpopulation depends on vesicular glutamate transporter 2 for mechanical pain, and together with substance P, inflammatory pain. Proc. Natl. Acad. Sci. USA *108*, 5789–5794.

Latremoliere, A., and Woolf, C.J. (2009). Central sensitization: a generator of pain hypersensitivity by central neural plasticity. J. Pain *10*, 895–926.

Leger, T., Grist, J., D'Acquisto, F., Clark, A.K., and Malcangio, M. (2011). Glatiramer acetate attenuates neuropathic allodynia through modulation of adaptive immune cells. J. Neuroimmunol. *234*, 19–26.

Li, S., Xue, C., Yuan, Y., Zhang, R., Wang, Y., Wang, Y., Yu, B., Liu, J., Ding, F., Yang, Y., and Gu, X. (2015). The transcriptional landscape of dorsal root ganglia after sciatic nerve transection. Sci. Rep. *5*, 16888.

Liou, J.T., Liu, F.C., Mao, C.C., Lai, Y.S., and Day, Y.J. (2011). Inflammation confers dual effects on nociceptive processing in chronic neuropathic pain model. Anesthesiology *114*, 660–672.

Lippoldt, E.K., Ongun, S., Kusaka, G.K., and McKemy, D.D. (2016). Inflammatory and neuropathic cold allodynia are selectively mediated by the neurotrophic factor receptor GFRα3. Proc. Natl. Acad. Sci. USA *113*, 4506–4511.

McKemy, D.D. (2011). A spicy family tree: TRPV1 and its thermoceptive and nociceptive lineage. EMBO J. *30*, 453–455.

Mishra, S.K., Tisel, S.M., Orestes, P., Bhangoo, S.K., and Hoon, M.A. (2011). TRPV1-lineage neurons are required for thermal sensation. EMBO J. *30*, 582–593.

Moalem, G., and Tracey, D.J. (2006). Immune and inflammatory mechanisms in neuropathic pain. Brain Res. Brain Res. Rev. *51*, 240–264.

Parikshak, N.N., Gandal, M.J., and Geschwind, D.H. (2015). Systems biology and gene networks in neurodevelopmental and neurodegenerative disorders. Nat. Rev. Genet. *16*, 441–458.

Pertin, M., Allchorne, A.J., Beggah, A.T., Woolf, C.J., and Decosterd, I. (2007). Delayed sympathetic dependence in the spared nerve injury (SNI) model of neuropathic pain. Mol. Pain *3*, 21.

Roberts, C.A., Dickinson, A.K., and Taams, L.S. (2015). The interplay between monocytes/macrophages and CD4(+) T cell subsets in rheumatoid arthritis. Front. Immunol. *6*, 571.

Rosas, M., Davies, L.C., Giles, P.J., Liao, C.T., Kharfan, B., Stone, T.C., O'Donnell, V.B., Fraser, D.J., Jones, S.A., and Taylor, P.R. (2014). The transcription factor Gata6 links tissue macrophage phenotype and proliferative renewal. Science *344*, 645–648.

Schuh, C.D., Pierre, S., Weigert, A., Weichand, B., Altenrath, K., Schreiber, Y., Ferreiros, N., Zhang, D.D., Suo, J., Treutlein, E.M., et al. (2014). Prostacyclin mediates neuropathic pain through interleukin 1β-expressing resident macrophages. Pain *155*, 545–555.

Sorge, R.E., Mapplebeck, J.C., Rosen, S., Beggs, S., Taves, S., Alexander, J.K., Martin, L.J., Austin, J.S., Sotocinal, S.G., Chen, D., et al. (2015). Different immune cells mediate mechanical pain hypersensitivity in male and female mice. Nat. Neurosci. *18*, 1081–1083.

Tegeder, I., Costigan, M., Griffin, R.S., Abele, A., Belfer, I., Schmidt, H., Ehnert, C., Nejim, J., Marian, C., Scholz, J., et al. (2006). GTP cyclohydrolase and tetrahydrobiopterin regulate pain sensitivity and persistence. Nat. Med. *12*, 1269–1277.

Vega-Avelaira, D., Géranton, S.M., and Fitzgerald, M. (2009). Differential regulation of immune responses and macrophage/neuron interactions in the dorsal root ganglion in young and adult rats following nerve injury. Mol. Pain *5*, 70.

Watkins, L.R., and Maier, S.F. (2002). Beyond neurons: evidence that immune and glial cells contribute to pathological pain states. Physiol. Rev. *82*, 981–1011.

Wijnvoord, N., Albuquerque, B., Häussler, A., Myrczek, T., Popp, L., and Tegeder, I. (2010). Inter-strain differences of serotonergic inhibitory pain control in inbred mice. Mol. Pain *6*, 70.

Xu, Z.Z., Kim, Y.H., Bang, S., Zhang, Y., Berta, T., Wang, F., Oh, S.B., and Ji, R.R. (2015). Inhibition of mechanical allodynia in neuropathic pain by TLR5-mediated A-fiber blockade. Nat. Med. *21*, 1326–1331.

Zhang, D.J., Wang, Q., Wei, J., Baimukanova, G., Buchholz, F., Stewart, A.F., Mao, X., and Killeen, N. (2005). Selective expression of the Cre recombinase in late-stage thymocytes using the distal promoter of the Lck gene. J. Immunol. *174*, 6725–6731.

Zhang, X., Wu, Z., Hayashi, Y., Okada, R., and Nakanishi, H. (2014). Peripheral role of cathepsin S in Th1 cell-dependent transition of nerve injury-induced acute pain to a chronic pain state. J. Neurosci. *34*, 3013–3022.

Zhu, X., Cao, S., Zhu, M.D., Liu, J.Q., Chen, J.J., and Gao, Y.J. (2014). Contribution of chemokine CCL2/CCR2 signaling in the dorsal root ganglion and spinal cord to the maintenance of neuropathic pain in a rat model of lumbar disc herniation. J. Pain *15*, 516–526.

Cell Reports, Volume *22*

Supplemental Information

Mechanistic Differences in Neuropathic Pain Modalities Revealed by Correlating Behavior with Global Expression Profiling

Enrique J. Cobos, Chelsea A. Nickerson, Fuying Gao, Vijayendran Chandran, Inmaculada Bravo-Caparrós, Rafael González-Cano, Priscilla Riva, Nick A. Andrews, Alban Latremoliere, Corey R. Seehus, Gloria Perazzoli, Francisco R. Nieto, Nicole Joller, Michio W. Painter, Chi Him Eddie Ma, Takao Omura, Elissa J. Chesler, Daniel H. Geschwind, Giovanni Coppola, Manu Rangachari, Clifford J. Woolf, and Michael Costigan

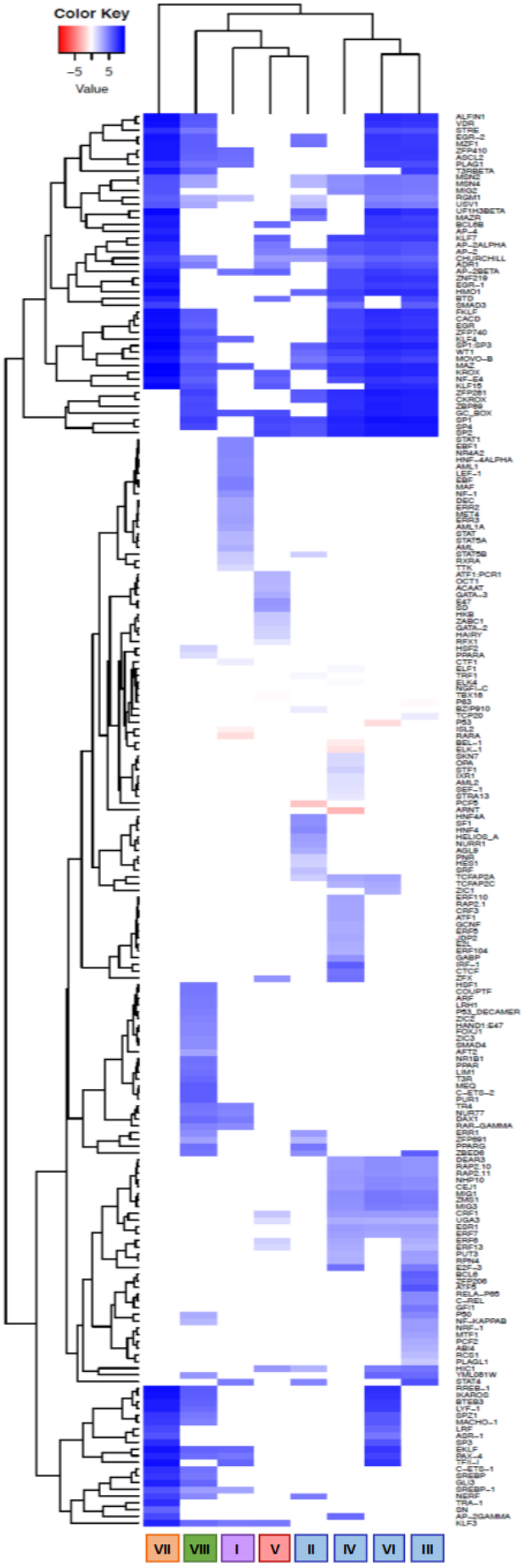

Figure S1 (Related to Figure 3). Transcription factor binding-site (TFBS) enrichment in each injury associated module. Heat map of 210 TFs (right margin) whose DNA-binding motifs were over-represented in the promoters of at least one gene cluster. Log-transformed raw enrichment score from clover algorithm was utilized for hierarchical clustering (Table S2). Hierarchical clustering of TFBS enrichment score for each cluster demonstrated the separation of neuronal and immune associated gene modules. Color code for gene clusters: Neuronal – Blue; Immune – Orange; Mixed – Green; Chemotaxis – Purple; Unknown – Red.

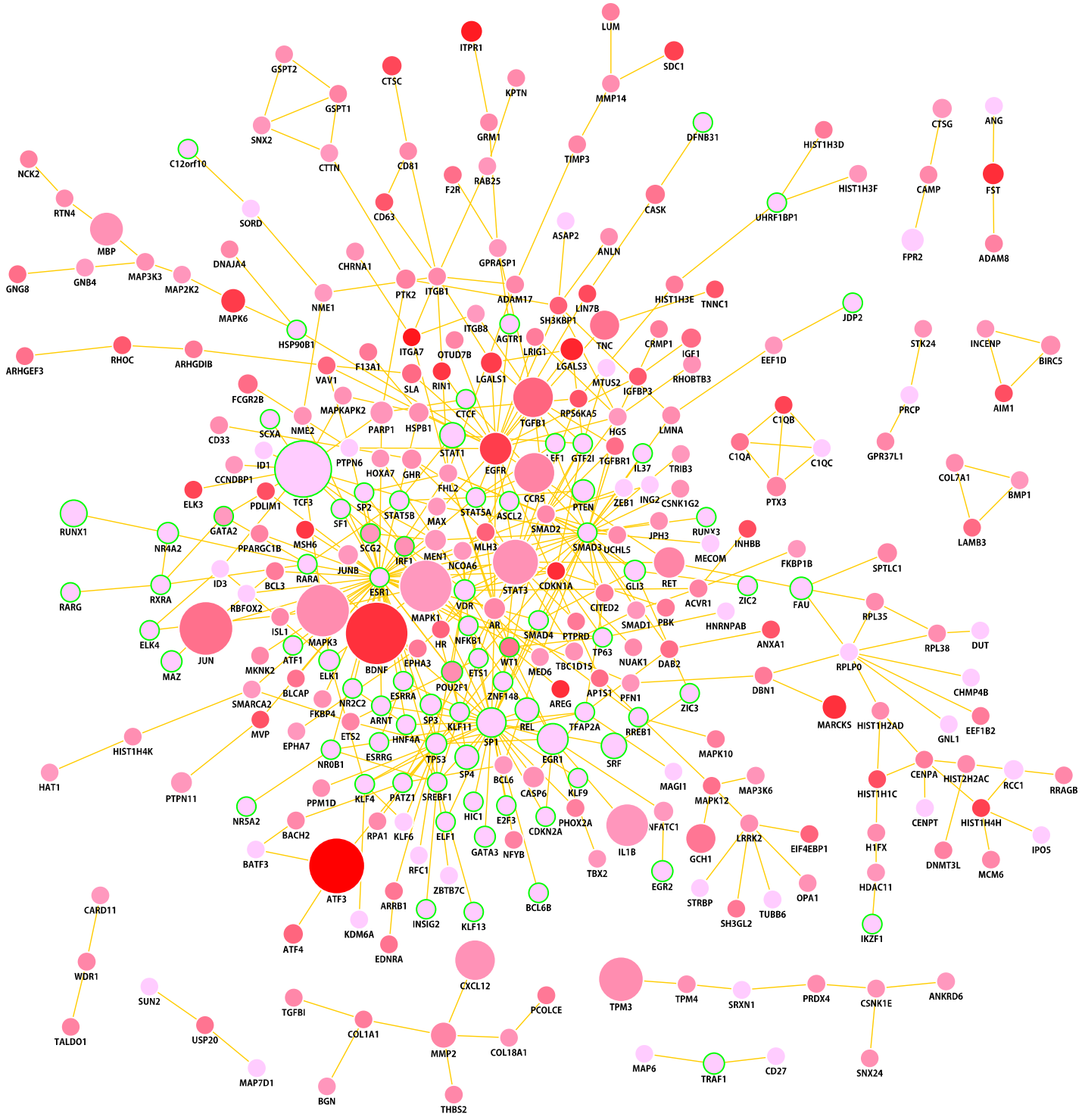

Figure S2 (Related to Figure 3). Protein-protein interaction network of genes differentially expressed in the DRG up to 10 post SNI nerve injury. Nodes correspond to genes and edges to protein-protein interaction (PPI). Over-represented TFs are encircled in green. Larger nodes correspond to number of PubMed hits with co-occurrence of gene and tactile allodynia, cold allodynia, neuropathic sensitivity or neuropathic pain tags. Nodes are colored based on their F-statistic values, pink to red (low to high).

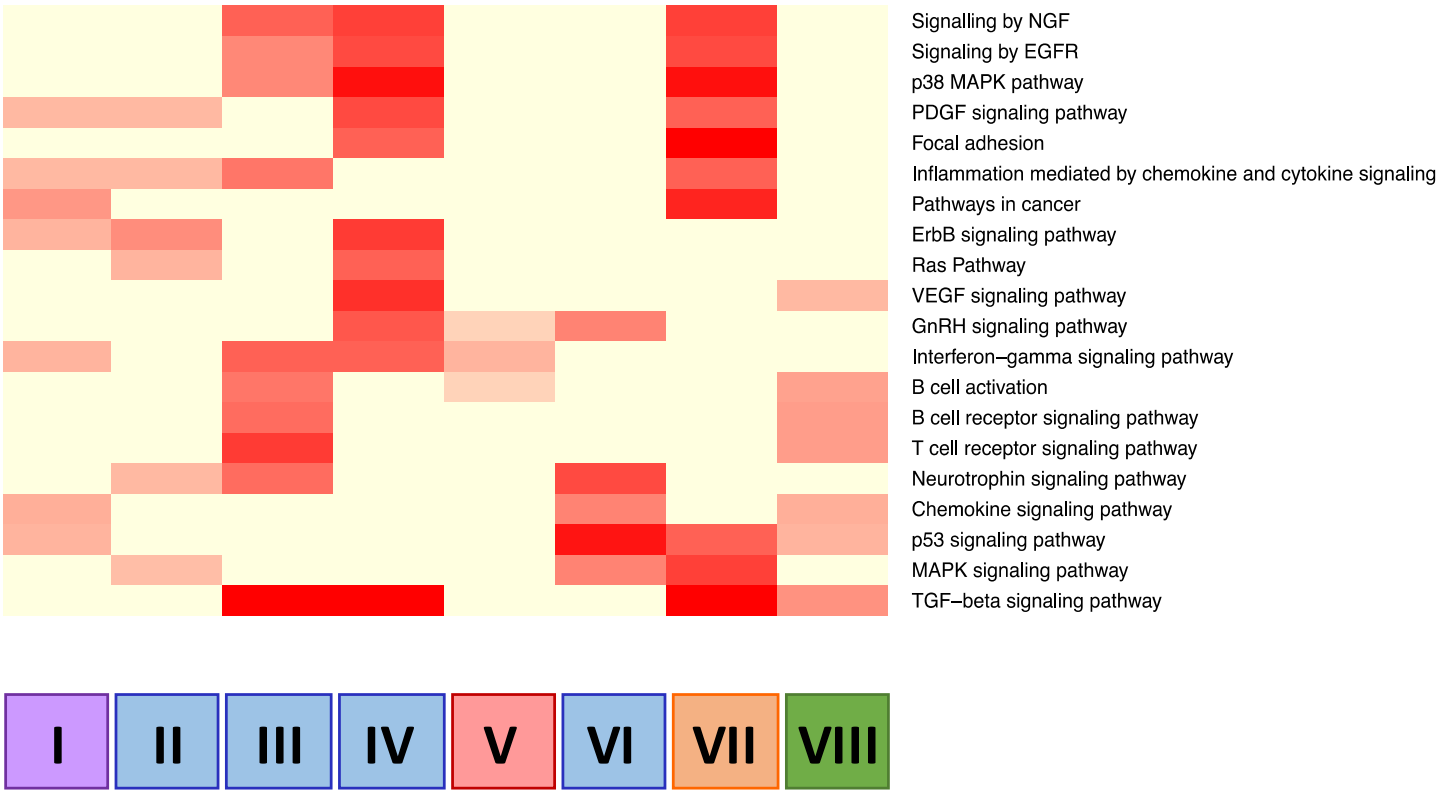

Figure S3 (Related to Figure 3). Signaling pathway enrichment analyses of neuropathic pain associated clusters. Heat map of twenty enriched pathways (Benjamini-corrected P-values < 0.05) in the PPI network and their association with eight neuropathic pain associated clusters are shown. Heat map are color-coded based on the percentage of individual pathway genes present in the corresponding neuropathic pain associated clusters (red is higher). Color code for gene clusters: Neuronal – Blue; Immune – Orange; Mixed – Green; Chemotaxis – Purple; Unknown –Red.

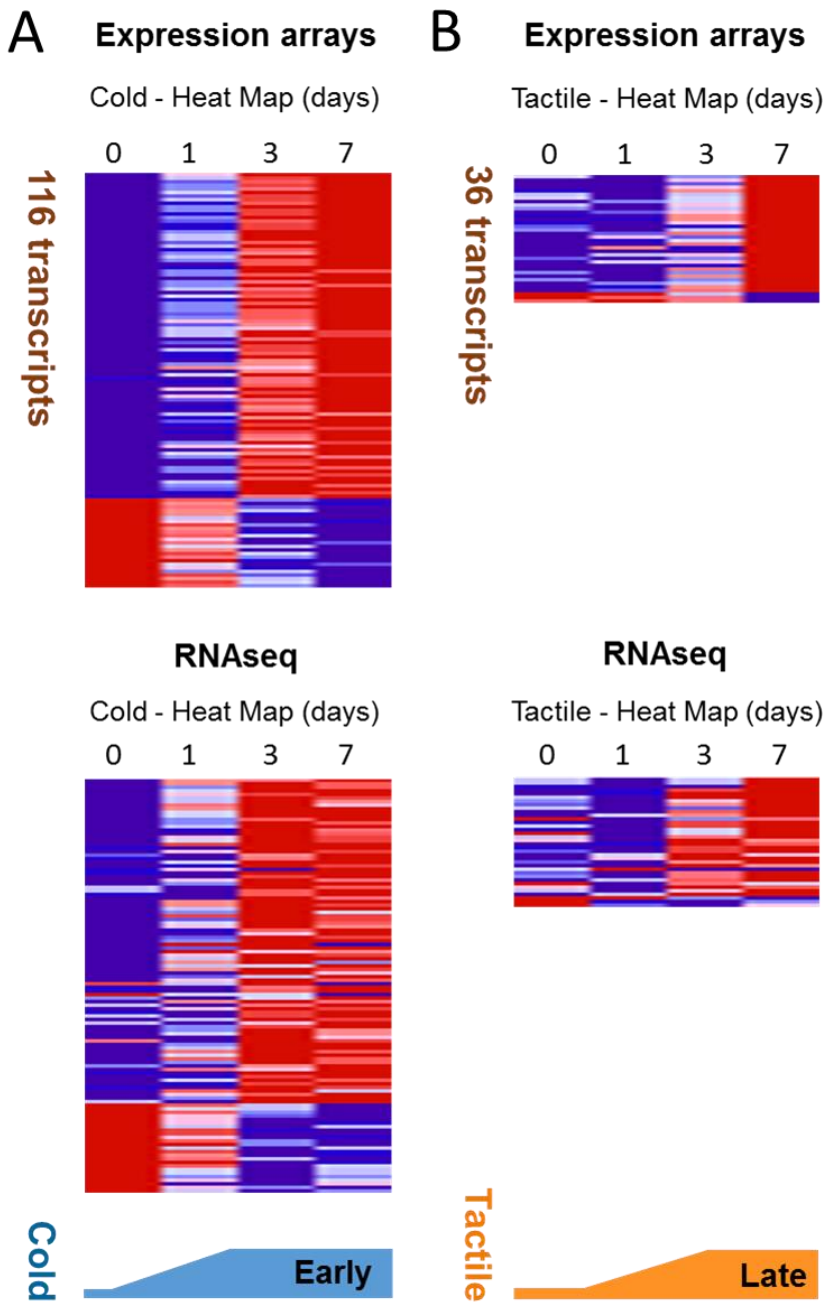

Figure S4 (Related to Figure 4). Expression heat maps of transcripts across four time points (Naïve, 1, 3, and 7 days post SNI). Common genes between the expression arrays and RNAseq data in each sensory modality (Cold and Tactile) are shown. These data demonstrate that the overall expression patterns of the constituent genes of each modality group were virtually identical regardless of the platform used to define the genes regulation. These data therefore act as a biological replicate of the expression groups used. The RNAseq data, as a whole, acts as a biological replicate of the entire data set. Heat map are color-coded based on the relative expression of individual transcripts (blue lower red higher expression). Color code for gene clusters: Cold – Blue; Immune – Orange.

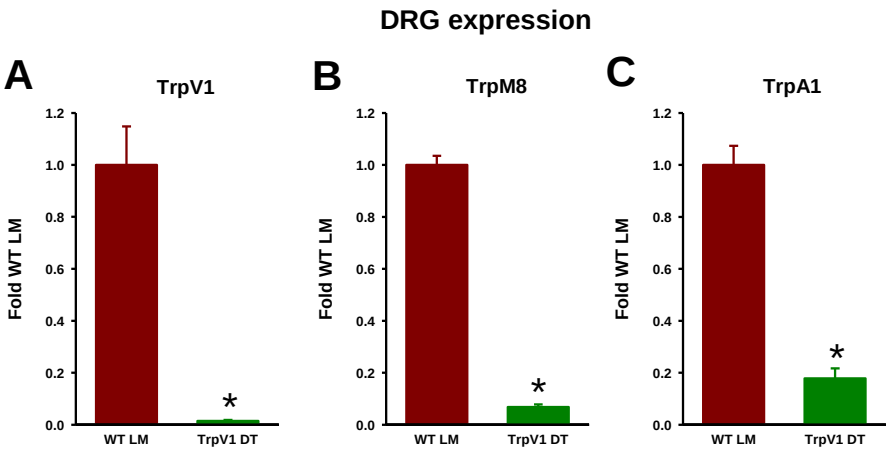

Figure S5 (Related to Figure 5). Expression of TrpV1, TrpM8 and TrpA1 in the DRG, determined by quantitative real-time PCR, from mice lacking TrpV1-lineage nociceptors (TrpV1 DTA) and in their wild-type littermate controls (WT LM). **(a)** TrpV1, **(b)** TrpM8 and **(c)** TrpA1 expression. Statistically significant differences between the values from both genotypes: **p<0.01 (unpaired Student's t-test). In all panels error bars indicate SEM.

Table S1 (Related to Figure 2). WGCNA analysis of all regulated transcripts in DRG. Significantly regulated probes across 10 days post SNI ($p<0.01$; moderated F-statistic, n=1704) were subject to WGCNA analysis to produce clusters of co-regulated transcripts, with no preconceived structure.

This table is provided as an Excel file.

Table S2 (Related to Figure 3). Analysis of transcription factor binding-sites (TFBS) enrichment. For estimation of TFBSs enrichment in the identified corresponding cluster-genelist promoter sequences (1000bp upstream from transcription start site), p-values were obtained relative to three background datasets: 1000bp of sequence upstream of all mouse gene, mouse CpG islands and mouse chromosome 19. Enriched TFBS position weight matrices from both JASPAR and TRANSFAC databases are provided in this table along with their clover enrichment score for each clusters.

This table is provided as an Excel file.

Table S3 (Related to Figure 3). Pathway analysis of the protein-protein interaction network from neuropathic pain associated clusters. For categorization and clustering of signaling pathway, we considered pathway terms with Benjamini-corrected p-values less than 0.05. The gene names and total number of genes present in each pathway are provided.

This table is provided as an Excel file.

Table S4 (Related to Figure 4). Correlation of the time course of neuropathic cold allodynia with transcript regulation in the DRG post SNI. The table shows the Pearson correlation coefficient as a measure of the degree of linear dependence between transcript regulation and sensory hypersensitivity. This parameter ranges from -1 (complete inverse correlation) through zero (no correlation) to 1 (maximal direct correlation). Probes are classified as up or downregulated based on the direct or inverse correlation with the increased neuropathic cold sensitivity. Absolute Pearson correlation indicates the absolute value of this parameter. Only those probes with an overall $p<0.01$ across the time course (moderated F-statistic) and an absolute Pearson correlation coefficient > 0.75 are shown.

This table is provided as an Excel file.

Table S5 (Related to Figure 4). Correlation of the time course of neuropathic tactile allodynia with transcript regulation in the DRG post SNI. The table shows the Pearson correlation coefficient as a measure of the degree of linear dependence between transcript regulation and sensory hypersensitivity. This parameter ranges from -1 (complete inverse correlation) through zero (no correlation) to 1 (maximal direct correlation). Probes are classified as down or upregulated based on the direct or inverse correlation with the decreased mechanical threshold during neuropathy. Absolute Pearson correlation indicates the absolute value of this parameter. Only those probes with an overall $p<0.01$ across the time course (moderated F-statistic) and an absolute Pearson correlation coefficient > 0.75 are shown.

This table is provided as an Excel file.

Table S6 (Related to Figure 4). Functional enrichment analysis using Ingenuity Pathway Analysis (IPA) software of the genes whose expression in the DRG correlates with neuropathic cold allodynia. Table shows selected functional annotations and their gene content. Analysis was performed on probes with an overall $p<0.01$ across the time course (moderated F-statistic) and an absolute Pearson correlation coefficient > 0.85.

Category	Function	Function Annotation	p-value	Genes
Neurological Disease	seizure disorder	seizure disorder	5.61E-05	AP1S1, C1QB, CA3, CACNA2D1, CITED2, GABRG1, GAL, ITPR1, NNAT, NPY, SCN4B, SLC6A4
Neurological Disease	ischemic stroke	ischemic stroke	2.29E-04	HIST2H2AA3/HIST2H2AA4, SLC6A4, VSNL1, XDH
Neurological Disease	Migraines	Migraines	3.15E-04	CA3, CACNA2D1, CX3CR1, GABRG1, SCN4B, SLC6A4
Neurological Disease	neuropathic pain	neuropathic pain	1.04E-03	CACNA2D1, KCNS1, SLC6A4

Table S7 (Related to Figure 4). Functional enrichment analysis using Ingenuity Pathway Analysis (IPA) software of the genes whose expression in the DRG correlates with neuropathic tactile allodynia. Table shows selected functional annotations and their gene content. Analysis was performed on probes with an overall $p<0.01$ across the time course (moderated F-statistic) and an absolute Pearson correlation coefficient > 0.85.

Category	**Function**	**Function Annotation**	**p-value**	**Genes**
Immunological Disease	systemic autoimmune syndrome	systemic autoimmune syndrome	1.06E-12	AIF1, C1QA, CCL4, CD74, CTSA, CX3CR1, CXCL16, HLA-DQB1, HLA-DRB5, LGALS1, LY6E, LYZ, MS4A7, RARRES2, TGFBI, TLR2, TYROBP
Cell-To-Cell Signaling and Interaction	activation	activation of antigen presenting cells	5.89E-11	CD74, CSF1R, CTSH, CX3CR1, HLA-DQB1, RARRES2, SLC11A1, TLR2, TREM2, TYROBP
Endocrine System Disorders	Diabetes - type 2	diabetes - type 2	7.86E-11	AIF1, CCL4, CD74, CX3CR1, CXCL16, HLA-DQB1, HLA-DRB5, LYZ, TGFBI, TLR2, TYROBP
Connective Tissue Disorders	rheumatoid arthritis	rheumatoid arthritis	1.82E-08	C1QA, CCL4, CD74, CXCL16, HLA-DQB1, HLA-DRB5, LGALS1, LYZ, MS4A7, RARRES2, TLR2

Table S8 (Related to Figure 4). Functional enrichment analysis using Gene Ontology (GO) software of the genes whose expression in the DRG correlates with neuropathic cold allodynia. Table shows selected functional annotations (GO terms) and their gene content. Analysis was performed on probes with an overall p<0.01 across the time course (moderated F-statistic) and an absolute Pearson correlation coefficient > 0.75.

Sno	Annotation	GO Terms	Count	%	p-value	Genes	List Total	Pop Hits	Pop Total	Fold Enrichment	Bonferroni	Benjamini	FDR
1	GOTERM_MF_FAT	GO:0042165~neurotransmitter binding	11	4.015	6.65E-07	GPR83, GABRG1, GABRG2, GLRB, CCKBR, CHRNA5, PROKR2, HTR3A, CHRNA1, HTR3B, NTSR2	200	87	13288	8.400	2.65E-04	2.65E-04	9.28E-04
2	GOTERM_MF_FAT	GO:0030594~neurotransmitter receptor activity	11	4.015	6.65E-07	GPR83, GABRG1, GABRG2, GLRB, CCKBR, CHRNA5, PROKR2, HTR3A, CHRNA1, HTR3B, NTSR2	200	87	13288	8.400	2.65E-04	2.65E-04	9.28E-04
3	GOTERM_CC_FAT	GO:0045202~synapse	19	6.934	1.06E-05	GABRG1, GABRG2, ACHE, GLRB, CPLX2, LIN7B, CASK, ITPR1, SEMA4F, CHRNA5, SV2B, LGI3, VAMP1, HTR3A, DOC2B, CHRNA1, HTR3B, GAP43, FAIM2	217	319	12504	3.432	0.0026	8.68E-04	0.0138
4	GOTERM_CC_FAT	GO:0044456~synapse part	14	5.109	7.99E-05	GABRG1, GABRG2, GLRB, LIN7B, ITPR1, SEMA4F, CHRNA5, LGI3, SV2B, CHRNA1, HTR3A, DOC2B, HTR3B, FAIM2	217	212	12504	3.805	0.0194	0.0049	0.1034
5	GOTERM_CC_FAT	GO:0045211~postsynaptic membrane	10	3.650	3.33E-04	GABRG1, GABRG2, GLRB, SEMA4F, CHRNA5, LIN7B, HTR3A, CHRNA1, HTR3B, FAIM2	217	126	12504	4.573	0.0783	0.0162	0.4301
6	GOTERM_MF_FAT	GO:0005230~extracellular ligand-gated ion channel activity	7	2.555	4.50E-04	GABRG1, GABRG2, GLRB, CHRNA5, HTR3A, CHRNA1, HTR3B	200	66	13288	7.047	0.1645	0.0353	0.6262
7	GOTERM_MF_FAT	GO:0015267~channel activity	16	5.839	3.98E-04	GABRG1, GABRG2, CACNA2D1, GLRB, AQP9, KCNK1, KCNIP1, ITPR1, FXYD7, KCNIP3, KCNS1, CHRNA5, SCN4B, HTR3A, CHRNA1, HTR3B	200	365	13288	2.912	0.1468	0.0389	0.5532
8	GOTERM_MF_FAT	GO:0022803~passive transmembrane transporter activity	16	5.839	3.98E-04	GABRG1, GABRG2, CACNA2D1, GLRB, AQP9, KCNK1, KCNIP1, ITPR1, FXYD7, KCNIP3, KCNS1, CHRNA5, SCN4B, HTR3A, CHRNA1, HTR3B	200	365	13288	2.912	0.1468	0.0389	0.5532
9	GOTERM_MF_FAT	GO:0005216~ion channel activity	15	5.474	7.90E-04	GABRG1, GABRG2, GLRB, CACNA2D1, KCNK1, KCNIP1, ITPR1, FXYD7, KCNIP3, KCNS1, CHRNA5, SCN4B, HTR3A, CHRNA1, HTR3B	200	349	13288	2.856	0.2703	0.0440	1.0954
10	GOTERM_MF_FAT	GO:0022838~substrate specific channel activity	16	5.839	3.48E-04	GABRG1, GABRG2, CACNA2D1, GLRB, AQP9, KCNK1, KCNIP1, ITPR1, FXYD7, KCNIP3, KCNS1, CHRNA5, SCN4B, HTR3A, CHRNA1, HTR3B	200	360	13288	2.953	0.1297	0.0452	0.4841

Table S9 (Related to Figure 4). Functional enrichment analysis using Gene Ontology (GO) software of the genes whose expression in the DRG correlates with neuropathic tactile allodynia. Table shows selected functional annotations (GO terms) and their gene content. Analysis was performed on probes with an overall p<0.01 across the time course (moderated F-statistic) and an absolute Pearson correlation coefficient > 0.75.

Sno	Annotation	GO Terms	Count	%	p-value	Genes	List Total	Pop Hits	Pop Total	Fold Enrichment	Bonferroni	Benjamini	FDR
1	GOTERM_BP_FAT	GO:0006955~immune response	18	18.750	6.54E-10	TLR2, VTN, H2-AB1, CCL4, TLR7, CLEC4N, RAET1B, TGFB1, FCGR3, C1QA, C1QB, SLC11A1, CXCL14, P2RY14, H2-EB1, CX3CR1, FCER1G, CD14	77	471	13588	6.744	7.22E-07	7.22E-07	8.15E-04
2	GOTERM_CC_FAT	GO:0005576~extracellular region	30	31.250	6.91E-07	GALNT2, RARRES2, CD109, VTN, CCL4, TGFB1, COL7A1, COMP, TGFBI, NMS, LOXL2, PLTP, VNN3, TNXB, LGALS1, MUP3, IGF1, F9, MMP14, C1QA, C1QB, BGN, NPY, CXCL14, NTS, CXCL16, LIPH, NPPB, COL1A1, TREM2	85	1680	12504	2.627	9.61E-05	9.61E-05	1.05E-06
3	GOTERM_BP_FAT	GO:0006954~inflammatory response	11	11.458	4.66E-07	C1QA, C1QB, SLC11A1, TLR2, NPPB, CCL4, TLR7, CD14, TGFB1, F2R, FCGR3	77	225	13588	8.627	5.1413E-04	2.57E-04	0.0007
4	GOTERM_CC_FAT	GO:0044421~extracellular region part	18	18.750	1.22E-05	TNXB, LGALS1, CD109, IGF1, VTN, MMP14, CCL4, TGFB1, BGN, COL7A1, CXCL14, NPY, CXCL16, COMP, TGFBI, COL1A1, LOXL2, VNN3	85	774	12504	3.421	0.0017	8.48E-04	0.0053
5	GOTERM_BP_FAT	GO:0009611~response to wounding	12	12.500	3.34E-06	C1QA, C1QB, SLC11A1, TLR2, NPPB, F9, CCL4, TLR7, CD14, TGFB1, F2R, FCGR3	77	347	13588	6.103	0.0037	9.20E-04	0.0104
6	GOTERM_BP_FAT	GO:0048584~positive regulation of response to stimulus	9	9.375	9.03E-06	C1QA, C1QB, SLC11A1, NPY, TLR2, UNC93B1, FCER1G, RAET1B, FCGR3	77	186	13588	8.539	0.0099	0.0012	0.0141
7	GOTERM_BP_FAT	GO:0050778~positive regulation of immune response	8	8.333	1.06E-05	C1QA, C1QB, SLC11A1, TLR2, UNC93B1, FCER1G, RAET1B, FCGR3	77	136	13588	10.380	0.0116	0.0013	0.0145
8	GOTERM_BP_FAT	GO:0001817~regulation of cytokine production	8	8.333	1.22E-05	SLC11A1, TLR2, FCER1G, TLR7, CD14, RAET1B, F2R, FCGR3	77	139	13588	10.156	0.0134	0.0013	0.0170
9	GOTERM_BP_FAT	GO:0019882~antigen processing and presentation	7	7.292	8.84E-06	SLC11A1, H2-EB1, UNC93B1, FCER1G, H2-AB1, RAET1B, FCGR3	77	87	13588	14.199	0.0097	0.0014	0.0196
10	GOTERM_BP_FAT	GO:0006952~defense response	13	13.542	6.51E-06	RARRES2, TLR2, TLR7, CCL4, TGFB1, FCGR3, C1QA, C1QB, SLC11A1, NPPB, FCER1G, CD14, F2R	77	448	13588	5.121	0.0072	0.0014	0.0304
11	GOTERM_BP_FAT	GO:0002684~positive regulation of immune system process	9	9.375	1.90E-05	C1QA, C1QB, SLC11A1, TLR2, UNC93B1, FCER1G, TGFB1, RAET1B, FCGR3	77	206	13588	7.710	0.0207	0.0017	0.4742

SUPPLEMENTAL EXPERIMENTAL PROCEDURES

Animals

Strains

Experiments were performed in adult (9-10 weeks old) male C57BL/6J mice (Jackson laboratory, Maine, USA). Heterozygous TrpV1-Cre (strain #017769) and heterozygous DTA stop animals (strain #010527) were bred together to produce TrpV1 DTA animals or non DTA expressing littermates. Rag1-null (strain #2216) were bred on a C57BL/6J background and backcrossed at least 10 times. To reveal T cell infiltration in the injured DRG we bred Lck-Cre (Jax #3802) with zsGreen reporter (Rosa-CAG-LSL-ZsGreen1-WPRE) (Jax #7906).

All studies performed in USA were conducted under strict review and guidelines according to the Institutional Animal Care and Use Committee (IACUC) at Boston Children's Hospital, which meets the veterinary standards set by the American Association for Laboratory Animal Science (AALAS). The experiments were reviewed and approved by the IACUC at Boston Children's Hospital under animal protocol numbers 15-04-2928R and 16-01-3080R. All experimental procedures performed in Spain were conducted in strict accordance to European standards (European Communities Council Directive 2010/63) and after approval of the animal protocols by regional (Junta de Andalucía) and institutional (Research Ethics Committee of the University of Granada, Spain) authorities. To decrease the number of animals in this study, we used the same mice for behavioral and in vitro studies, when possible.

Spared nerve injury

Mice were anesthetized with isoflurane (2–4%) and SNI surgery performed; the tibial and common peroneal branches of the sciatic nerve were tightly ligated with a silk suture and transected distally while the sural nerve was left intact (Bourquin et al., 2006; Decosterd and Woolf, 2000). In sham-operated controls, the sciatic nerve terminal branches were exposed but not ligated. Wounds were closed and the animals returned to their cages.

Immune cell depletion or reconstitution

To deplete macrophages *in vivo*, we administered 100 µl of anionic liposome-encapsulated clodronate i.v. 24h before SNI surgery (Clophosome-ATM, FormuMax Scientific, Sunnyvale, CA), into the tail vein of mice under isofluorane anesthesia (Kobayashi et al., 2015). Liposomes devoid of clodronate were used as a control.

For *Rag1*$^{-/-}$ reconstitution experiments, $CD4^+$ and $CD8^+$ T cells were enriched from male C57BL/6J splenic and lymph node single cell suspensions using magnetically labeled anti-CD4 and anti-CD8α microbeads (Miltenyi). 5 x 10^6 $CD4^+$ and 2.5 x 10^6 $CD8^+$ T cells were injected into the tail veins of male *Rag1*$^{-/-}$ recipients. SNI surgeries were performed 16 days after transfer. Reconstitution of T cell compartments was assessed by flow cytometry on peripheral blood mononuclear cells using antibodies (Biolegend) to CD4, CD8α and B220 (to detect B cells). Flow cytometry data were collected on an LSR II analyzer (BD Biosciences) and analyzed using FlowJo software (Treestar).

Behavioral tests

Measures of mechanical and cold allodynia

A time course of tactile and cold sensitivity before and after SNI was measured in C57BL/6J mice. Animals were acclimated for two hours in test compartments (7.5 cm wide x 7.5 cm long x 15 cm high) placed on an elevated mesh-bottomed platform, to access to ventral hind paws. Two groups of mice (n=13 or 14 per group) were assayed every other day prior to and post SNI. One group was used to determine baseline 1 (BL1) then 1, 3, 5, 7, 9 and 14 days post SNI, the second was used to assay baseline 2 (BL2) then 2, 4, 6, 8, 10 and 15 days post SNI. Each group was assayed every other day to prevent animals becoming over stimulated and/or habituated to the testing. Both groups exhibited sensitivity changes that altered in a consistent fashion over the time course. Mechanical allodynia was measured using von Frey filaments (Touch-Test Sensory Evaluators; North Coast Medical Inc., Gilroy, CA) ranging from 0.07 to 2 g. Filaments were applied for 2-3 s to the sural territory of the hind paw plantar surface using the up–down paradigm (Chaplan et al., 1994). Evaluation was initiated with a 0.6-g von Frey filament. In each consecutive test, if there was no response to the filament, a stronger stimulus was then selected; if there was a positive response, a weaker one was then used. The response to the filament was considered positive if immediate licking/biting, flinching or fast withdrawal of the stimulated paw was observed.

Cold allodynia was assayed by applying a 10µl drop of acetone to the hind paw ipsilateral to the SNI injury and measuring the amount of time the animal spent flinching/licking/biting the paw in seconds. TrpV1 DTA mice were tested twice at baseline and then 7, 14 and 21 post SNI. Macrophage depleted mice were tested at baseline and on days 7, 10, 14 and 21 post SNI. Rag1 -/- and T cell addition mice were tested at baseline twice, again post T cell addition, and then 7, 14, 21 and 28 post SNI.

As mice subject to SNI develop exquisite hypersensitivity over the first week following nerve injury and this study relies on the careful determination of its onset, we took special care not to introduce any confounds in evaluating the sensitivity. For measuring tactile allodynia we took special care to reduce the effects of repeated measures that occur with repetitive von Frey stimulation, by leaving at least 30 seconds between every stimulation. When testing cold allodynia we ensured that only the acetone touched the hind paw.

All experiments were performed in at least two independent sets of mice.

Dynamic Thermal Place Aversion Test – Naïve TrpV1 DTA animals

Two thermal plates were placed directly adjacent to one another with a plastic chamber surrounding both allowing free movement between each plate (Bioseb, France). The temperature of each plate was set to continuously change by 1.05 degrees Celsius per minute. At the start of the experiment plate A was set at 4ºC (noxious cold) the alternate plate was set to 25ºC (ambient). The gradient of temperature change was equal on both plates but opposite, so as plate A's temperature rose toward 25ºC the alternate plate's temperature was reduced toward 4ºC with this half-cycle complete in 22 minutes. Once these temperatures had been reached, the direction of the temperature change for each plate was reversed, so that plate A now returned back to 4ºC and B to 25ºC to complete the cycle. Constantly moving the plate temperatures is required to prevent the animals settling in the ambient option. The time spent in each plate was automatically recorded at 30 s intervals using Ethovison XT v11.5 video-tracking software (Noldus, Netherlands). Experiments were performed in at least two independent sets of mice.

Data analysis of behavioral studies

Statistical analysis was carried out with a one-way or two-way repeated measures analysis of variance (ANOVA), followed by a Bonferroni post-hoc test in all cases. The differences between values were considered significant when the p-value was below 0.05. The data were analyzed with SigmaPlot 12.0 software (Systat Sofware Inc, CA, USA).

RNA analysis

RNA preparation

We studied DRGs collected in three biological replicates every 8 hours from the time of SNI until 24 hours post injury, and then daily until 10 days. Total RNA was extracted from naive and injured DRGs (ten ipsilateral L4/5 DRGs per sample, five mice) using Trizol reagent (Fisher Biotech) and standard methods. Total RNA quality evaluated with the Agilent Bioanalyzer (Agilent Technologies).

For RNAseq three biological replicates distinct to those collected above were assayed. Total RNA was extracted from naive and injured DRGs (six ipsilateral L4/5 DRGs per sample, three mice) using Trizol as above.

Microarray-based gene expression analysis

Total RNA (200 ng) was amplified, biotinylated, and hybridized to 40 Illumina MouseRef-8 v2.0 Expression BeadChips. Raw data were analyzed using Bioconductor packages (www.bioconductor.org).

Additional biologically independent groups of naive uninjured DRGs (n=7) were assayed to increase the accuracy of the baseline reference values. Clustering based on top variant genes was used to assess overall data coherence. The inter-array Pearson correlation across all probes between each array and all others was used to identify outliers, defined as having an average Pearson correlation >2 standard deviations away from the mean. Four outliers were excluded from the analysis, and data renormalized after outlier exclusion.

Contrast analysis of differential expression was performed using the LIMMA package (Smyth, 2005) After linear model fitting, we calculated 1) a Bayesian estimate of differential expression (moderated t-statistic) for all comparisons; and 2) an overall moderated F-statistic (F) combining the t-statistics for all the contrasts into an overall test of significance. The moderated F-statistics is similar to the ordinary F-statistic from analysis of variance except that the denominator mean squares are moderated across genes (https://www.bioconductor.org/packages/devel/bioc/vignettes/limma/inst/doc/usersguide.pdf). The threshold for statistical significance was set at $p<0.005$ for individual comparisons and at $p<0.01$ across the time course. Only transcripts significant in the moderated F-statistics were used for further analyses (1704 probes). Expression data from microarray can be found in GEO (accession number GSE102937).

RNAseq-based gene expression analysis

The samples were sequenced by the UCLA Neuroscience Genomics Core. RNA-sequencing was carried out using Nugen Ovation RNA Ultra Low Input (500 pg) + TruSeq Nano and then sequenced at 69bp paired end reads. The paired end sequencing reads were aligned to mouse genome (mm10) using aligner STAR with default parameters, read counts were obtained with HTSeq-count. Differential expression analyses were performed with software R and Bioconductor packages of edgeR and limma voom. GEO accession number (GSE102937).

Q-PCR-based gene expression analysis

Ipsilateral L4/L5 DRGs were harvested and RNA extracted by acid phenol extraction (TRIzol reagent, Invitrogen). First-stranded cDNA synthesis (1 µg of total RNA per reaction) was performed with SuperScript III Reverse Transcriptase (Invitrogen). Quantitative real-time PCR was performed using the Sybr green detection system with primer sets designed using the Primer Blast algorithm (NCBI), primer pairs were designed to span an intron whenever possible. Specific PCR product amplification was confirmed using the amplicon dissociation protocol. Transcript regulation was determined using the relative standard curve method (Applied Biosystems). Relative loading was determined before RT with RNA spectrophotometry followed by gel electrophoresis and after RT by amplification of glyceraldehyde-3-phosphate dehydrogenase. We tested the DRG expression of TrpV1, TrpM8 and TrpA1 in TrpV1 DT mice and their wild-type LM controls, and the expression of the macrophage markers CD68, Iba1 and CD163 in liposome controls- and clodronate-treated mice. Values were compared using an unpaired Student's t test using SigmaPlot 12.0 software (Systat Sofware Inc).

Bioinformatics

Weighted Gene Co-Expression Network Analysis

To facilitate identification of gene modules (groups of highly co-expressed genes), we constructed a weighted gene co-expression network (WGCNA) using the regulated transcripts. Briefly, we computed the absolute Pearson correlation coefficients between each probe and every other probe in the expression dataset; these values were used to determine the topological overlap, a measure of connection strength, or 'neighborhood sharing', in the network. This resulted in modules of highly co-expressed genes where the members of each network have high topological overlap in their temporal patterns of regulation (Horvath et al., 2006; Oldham et al., 2008; Parikshak et al., 2015). Heat maps were generated using HetMapImage tool from GenePattern software (v. 3.9.10).

Sensory Modality Expression Correlations

To correlate expression over time of genes defined as regulated with the temporal changes in behavioral hypersensitivity we used the Pearson correlation coefficient as a measure of the degree of linear dependence between transcript regulation and sensory hypersensitivity. This parameter ranges from -1 (complete inverse correlation) through zero (no correlation) to 1 (maximal direct correlation). Both direct and inverse correlation coefficients were used to define genes whose expression changes were similar to pain-like hypersensitivity changes over time.

RNAseq based Expression Correlations

To biologically validate the sensory modality results, we tested whether the transcripts within sensory modality group showed a similar regulation profile using RNAseq data from independent tissue samples. We selected all common transcripts in both platforms within each gene cluster and compared the resulting heat maps. Heat maps were generated as above.

Functional Enrichment Analyses

To initially identify functional categories heavily represented within either each gene expression cluster (from the WGCNA analysis) or behavioral sensory modality correlated transcript group (from the Pearson hypersensitivity correlated lists) we analyzed each gene list with Ingenuity Pathway Analysis (IPA) software, version 9.0 (Qiagen, USA). As a second method to determine cellular functions predominant in the pain modality correlated gene lists, we employed the Gene Ontology (GO) software (http://geneontology.org/). For the IPA based gene list / functional pathway correlations we used a Pearson cut off of 0.85 (±); for GO based gene list / gene function correlations we used a relatively less restrictive Pearson 0.75 (±) cut off. A lower threshold was used for the GO analysis because this algorithm performs better with more transcripts in the gene lists than the IPA algorithm which loses specificity at lower thresholds.

In addition to these two gene function predicting algorithms we chose to independently assay the content of each gene group (WGCNA expression cluster or Pearson behavior correlate) by comparing them to two gene expression sets from the literature. To represent DRG neurons we used a nociceptor specific gene expression set, obtained from FACS isolated Nav1.8 positive DRG neurons from the mouse (GSE46546 (Chiu et al., 2014)). Nav1.8 is expressed in about 80% of total DRG neurons, including a large proportion of C-fibers and

a smaller population of medium-sized myelinated cells, and therefore this set includes the signature of nociceptive neurons. To represent resident and infiltrating immune cells in the DRG post nerve injury we used a mouse activated macrophage expression set (GSE28621, F4/80+, CD11b+ inflammation-associated macrophages 72 hours post stimulation, from (Rosas et al., 2014)). To represent activated T cells we used a mouse Th1 polarized T cell expression set (GSE60354, DNRAR_YFP_IFNG Interferon stimulated T cells, from (Brown et al., 2015)). These leukocyte subsets represent a large proportion of the immune cells in the DRG after nerve injury (Hu and McLachlan, 2002).

Transcription factor binding site enrichment

Transcription factor binding site (TFBS) enrichment analysis was performed by scanning the canonical promoter region (1000bp upstream of the transcription start site) for the genes present in all eight clusters. Next we utilized TFBS position weight matrices (PWMs) from JASPAR (205 non-redundant and experimentally defined motifs) and TRANSFAC (2,208 redundant, manually curated database, extracted from the original scientific literature motifs) databases (Matys et al., 2003; Portales-Casamar et al., 2010) to examine the enrichment for corresponding TFBS within each cluster. For TFBS enrichment all the cluster were scanned with each PWMs using Clover algorithm (Frith et al., 2004). To compute the enrichment analysis we utilized three different background datasets (1000 bp sequences upstream of all mouse genes, mouse CpG islands and mouse chromosome 19 sequence), and the TFs were considered significant when $p<0.05$ relative to all 3 background/control datasets.

Protein-Protein Interaction (PPI) network analyses

We constructed an experimentally validated protein–protein interaction (PPI) network using all the genes present in the eight clusters. We created all possible combinations of gene pairs present in these clusters and identified all experimentally verified interaction data (in humans dataset) for their corresponding proteins in the STRING database (integration of the following databases: BIND, DIP, GRID, HPRD, IntAct, MINT, and PID) (Franceschini et al., 2013), constructing the protein network by force-directed layout using edge betweenness. The size of each node in the PPI network is determined by its corresponding protein's literature association with neuropathic pain. For that we determined the association with the following key-words: tactile allodynia, cold allodynia, neuropathic sensitivity or neuropathic pain in the PubMed database for every protein using R (http://cran.r-project.org/).

FACS

Briefly, total blood, and ipsilateral L3-5 DRGs were harvested from Liposome or Clodronate treated animals following nerve injury. For blood, red cells were lysed using red blood cell lysis buffer (Sigma). DRG's were digested in collagenase/dispase for 1hr at 37C, gently dissociated, and stained with the following antibodies (all from eBioscience, clone designations in parentheses): CD45 (30-F11), CD3 (145-2C11), CD11b (M1/70), CD11c (N418) and Siglec-F (1RNM44N). All samples were pre-incubated with anti-CD16/32 to block Fc receptors. Samples were read using a BD LSRFortessa.

T cell Labeling and Macrophage Immunostaining

On day 7 after surgery, SNI mice treated with clodronate or its vehicle were anesthetized with isoflurane 3% (Braun VetCare, Barcelona, Spain) in oxygen and transcardially perfused with 0.9% saline solution followed by 4 % paraformaldehyde with 1.5 % picric acid in 0.1 M phosphate buffer (pH 7.4). L4 ipsilateral DRGs were excised, post-fixed one hour 4 °C in the same fixative solution, cryoprotected for 48 h at 4 °C in 30% sucrose (Sigma-Aldrich, Madrid, Spain) in water, embedded in optimal cutting temperature embedding compound (O.C.T., Sakura Tissue-Tek, CA, USA) and frozen at −80 °C. Longitudinal DRG sections were serially cut in a cryostat at 15 µm and thaw-mounted onto microscope slides (Sigma-Aldrich). Slides were washed in TBST (tris-buffered saline with Tween 20 [0.1%]) and incubated in a blocking solution containing 5% normal goat serum (Jackson Immuno Research, PA, USA) in TBST for 1 hour at room temperature (RT) and then incubated at 4 °C overnight with an anti-IBA1 (1:1000, Wako, Japan) as a marker of macrophages/monocytes. Following primary antibody incubation, the tissue sections were washed and incubated for 1 h (RT) with secondary antibody solution containing goat anti-rabbit Alexa Fluor 488 (1:500, Life Technologies, Carlsbad, CA, USA). Antibody solutions were prepared in TBST with 5% normal goat serum and 0.3% Triton X-100 (Sigma-Aldrich). Slides were coverslipped with ProLong® Gold Antifade mounting medium (Molecular Probes; Oregon, USA) and visualized under an fluorescente microscope (Nikon Eclipse Ti, Nikon Instruments Inc., Melville, NY, USA) and processed with Image-J software (version 1.48, Wayne Rasband, NIH, Bethesda, MD, USA). To reveal T cell infiltration in the injured DRG we bred Lck-Cre (Jax #3802) with zsGreen reporter (Rosa-CAG-LSL-ZsGreen1-WPRE) (Jax #7906), and followed the same procedure described above but using a secondary antibody solution containing goat anti-rabbit Alexa Fluor 594 (1:500, Life Technologies, Carlsbad, CA, USA) to label the primary anti-IBA1. These animals express the strong florescent green marker in activated T cells.

SUPPLEMENTAL REFERENCES

Bourquin, A.F., Suveges, M., Pertin, M., Gilliard, N., Sardy, S., Davison, A.C., Spahn, D.R., and Decosterd, I. (2006). Assessment and analysis of mechanical allodynia-like behavior induced by spared nerve injury (SNI) in the mouse. Pain 122, 14 e11-14.

Chaplan, S.R., Bach, F.W., Pogrel, J.W., Chung, J.M., and Yaksh, T.L. (1994). Quantitative assessment of tactile allodynia in the rat paw. Journal of neuroscience methods 53, 55-63.

Franceschini, A., Szklarczyk, D., Frankild, S., Kuhn, M., Simonovic, M., Roth, A., Lin, J., Minguez, P., Bork, P., von Mering, C., and Jensen, L.J. (2013). STRING v9.1: protein-protein interaction networks, with increased coverage and integration. Nucleic acids research 41, D808-815.

Frith, M.C., Fu, Y., Yu, L., Chen, J.F., Hansen, U., and Weng, Z. (2004). Detection of functional DNA motifs via statistical over-representation. Nucleic acids research 32, 1372-1381.

Horvath, S., Zhang, B., Carlson, M., Lu, K.V., Zhu, S., Felciano, R.M., Laurance, M.F., Zhao, W., Qi, S., Chen, Z., et al. (2006). Analysis of oncogenic signaling networks in glioblastoma identifies ASPM as a molecular target. Proceedings of the National Academy of Sciences of the United States of America 103, 17402-17407.

Matys, V., Fricke, E., Geffers, R., Gossling, E., Haubrock, M., Hehl, R., Hornischer, K., Karas, D., Kel, A.E., Kel-Margoulis, O.V., et al. (2003). TRANSFAC: transcriptional regulation, from patterns to profiles. Nucleic acids research 31, 374-378.

Oldham, M.C., Konopka, G., Iwamoto, K., Langfelder, P., Kato, T., Horvath, S., and Geschwind, D.H. (2008). Functional organization of the transcriptome in human brain. Nature neuroscience 11, 1271-1282.

Portales-Casamar, E., Thongjuea, S., Kwon, A.T., Arenillas, D., Zhao, X., Valen, E., Yusuf, D., Lenhard, B., Wasserman, W.W., and Sandelin, A. (2010). JASPAR 2010: the greatly expanded open-access database of transcription factor binding profiles. Nucleic acids research 38, D105-110.